12-2016

Interactive Physics and Characteristics of Photons and Photoelectrons in Hyperbranched Zinc Oxide Nanostructures

Garrett Edward Torix
University of Arkansas, Fayetteville

Interactive Physics and Characteristics of Photons and Photoelectrons in Hyperbranched Zinc Oxide Nanostructures

A thesis submitted in partial fulfillment
of the requirements for the degree of
Master of Science in Microelectronics-Photonics

by

Garrett Torix
Henderson State University
Bachelor of Science in Physics, 2014

December 2016
University of Arkansas

This thesis is approved for recommendation to the Graduate Council.

Dr. Ryan Tian
Thesis Director

Dr. Joseph Herzog
Committee Member

Dr. Shui-Qing Yu
Committee Member

Dr. Rick Wise
Ex-Officio Member

The following signatories attest that all software used in this thesis was legally licensed for use by Garrett Torix for research purposes and publication.

Mr. Garrett Torix, Student	Dr. Ryan Tian, Thesis Director

This thesis was submitted to http://www.turnitin.com for plagiarism review by the TurnItIn company's software. The signatories have examined the report on this thesis that was returned by TurnItIn and attest that, in their opinion, the items highlighted by the software are incidental to common usage and are not plagiarized material.

Dr. Rick Wise, Program Director	Dr. Ryan Tian, Thesis Director

Abstract

As is commonly known, the world is full of technological wonders, where a multitude of electronic devices and instruments continuously help push the boundaries of scientific knowledge and discovery. These new devices and instruments of science must be utilized at peak efficiency in order to benefit humanity with the most advanced scientific knowledge. In order to attain this level of efficiency, the materials which make up these electronics, or possibly more important, the fundamental characteristics of these materials, must be fully understood. The following research attempted to uncover the properties and characteristics of a selected family of materials. Herein, zinc oxide (ZnO) nanomaterials were investigated and subjected to various, systematical tests, with the aim of discovering new and useful properties. The various nanostructures were grown on a quartz substrate, between a pair of gold electrodes, and subjected to an electrical bias which produced a measurable photocurrent under sufficient lighting conditions. This design formed a novel photodetector device, which, when combined with a simple solar cell and a methodical set of experimental trials, allowed several unique phenomena to be studied. Under various conditions, the device photocurrent as a function of applied voltage, as well as transmitted light, were measured and compared between devices of different ZnO morphologies. Zinc oxide is an absorber of ultraviolet (UV) light. UV absorbing materials and devices have uses in solar cells, long range communications, and astronomical observational equipment, hence, a better understanding of zinc oxide nanostructures and their properties can lead to more efficient utilization of UV light, improved solar cell technology, and a better understanding of the basic science in photon-to-electricity conversion.

Acknowledgements

Firstly, I would like to acknowledge my research advisor, Dr. Ryan Tian, who graciously and excitably accepted me into his research group. He gave me full access to his lab, resources, and mentored and guided me through the initial research which became the material for this thesis. Dr. Tian's knowledge and guidance has aided me throughout my whole graduate school career.

Secondly, I would like to acknowledge Dr. Rick Wise, who has been an exceptional program director, graduate school advisor, and friend to me these past couple of years.

Dedication

This thesis and the many hours of work put into it is dedicated to my wonderfully supportive wife, Julie Torix, who has stood by my side all through graduate school and helped keep me mentally focused. You have helped me carry and push through the stress school has challenged me with for two and a half years, and this work would not have been completed without you.

This work is also dedicated to my parents, Eddie and Holly Torix, who have spent much of their lives raising me and helping me get to where I am today.

Table of Contents

Table of Figures

1. Introduction

1.1. Research Motivation

The origins of the thesis research began with an investigation into an UV photocatalyst; specifically, by exploring the use of semiconducting zinc oxide to split water molecules into hydrogen and oxygen. A more efficient method for generating these gases could help lead the way toward cheaper, clean fuel. Hyperbranched ZnO nanostructures were grown onto a quartz slide, between two gold electrodes, forming a simple photodetector which, when an external voltage was passed through, would split the water molecules. During the experimentation process, some unusual and interesting electrical characteristics of the UV-detector were observed. On this basis, a secondary set of experiments were started and designed to investigate the fundamental origins of these abnormal phenomena and their links to interactions between matter (zinc oxide), photons, and energy (photoelectrons) under various experimental conditions.

The investigation uncovered additional properties of the photodetector and zinc oxide, which will be discussed later in this thesis. Thus, the goals which motivated the previous experiment shifted towards optimizing the absorption and detection of UV radiation as a means to uncover the causes of the phenomena mentioned previously. It was believed that by subjecting the zinc oxide ultraviolet photodetector to a series of systematic experimental conditions, a conclusion about the nature of the observed phenomena could be drawn, and the material properties, such as photon absorption and current generation, could be better controlled and optimized. This optimization could lead to improved electronics such as solar cells or photodetection devices, like those used in high-tech telescopes. Improved solar cells can help shift humanity's dependence from fossil fuels towards cheap, renewable resources; while more

efficient UV absorbers have the potential to improve the resolution of astronomical images and increase humanity's understanding of the universe.

1.2. Review of Relevant Scientific Principles

1.2.1. Basic Semiconductor Operation

Semiconducting materials are those which are not entirely conductors or insulators, or in other words, their electronic conductivity is not constant. Semiconductor conductivity is influenced by the number of available mobile charge carriers in the material, which can change based off several variables. Mobile charge carriers are defined as being free, or unbound by the atoms within the semiconductor lattice, and can be either negatively charged electrons or positively charged holes. These mobile carriers can be generated by increasing the temperature of the material, doping other elements into the lattice, and through the absorbance of a specific wavelength of photons by the atoms within the lattice.

The electrons, which orbit the billions of atoms within a semiconductor's lattice, each have their own energy levels, and when they are in proximity to a multitude of other electrons and their own respective energy levels, they form what is called an energy band and a corresponding energy band gap. The energy band gap represents a range of electron energy levels in which no electrons reside. Below the band gap is the valence band, and above is the conduction band. At zero Kelvin, all the electrons in an ideal semiconductor are located within the valence band. Once energy is added into the material, typically in the form of heat, the electrons will absorb the energy, become excited, and "jump" from the valence band to the conduction band, as mobile negative charge carriers. When an electron moves from the valence to conduction band, it leaves an orbital level which then has one less electron, and, thus is positively charged. This positively charged "space" is referred to as a hole, and acts as a mobile charge carrier which moves

opposite the electrons. In the presence of an external electric field, the charge carriers will react to the force and drift about the lattice, electrons in one direction along the field, and holes in the other.

The energy band gap varies in size from one semiconducting material to another, requires difference values of energy to jump from the valence to the conduction band, and depends on the atoms within the lattice and the number and energy of electrons orbiting them. Doping, which refers to the addition of other atoms into a pure semiconductor (such as boron into a silicon lattice), can introduce energy levels which are within the band gap and can aid electrons in their "jump" across the gap. Doping also has the effect of adding extra charge carriers into the lattice, either by releasing an extra electron or pulling one from another atom, which then leaves behind a positive hole. These additions increase the conductivity of the semiconductor. Besides a change in energy, electrons may also need a change in another property before the jump across the energy band gap can be made: momentum. If an energy band gap requires a change in energy and momentum, it is called an indirect band gap. Direct band gaps only require a sufficient change in electron energy to make the jump [1-3].

1.2.2. Metal-semiconductor Characteristics

The research which this paper details involved the use of a zinc oxide photodetector. Metal-semiconductor contacts were utilized in order to apply an electrical potential across the device. Certain characteristics arise when a metal material and semiconductor come in physical or electrical contact. The respective energy levels of the two materials will evolve in response to the contact. Prior to contact, the energy levels of a n-type semiconductor and a metal resemble what is shown in Figure 1.1. The electron energy levels of the two materials are compared via their distances away from the vacuum level, which is the energy level of a completely free,

unbound by the lattice, electron. The energy level of the semiconductor valence and conduction band, as well as the Fermi energies of both materials are shown by E_V, E_C, and E_F, respectively. The Fermi energy level is defined as the energy value at which the chance of finding an electron is exactly fifty percent. At zero Kelvin, in a pure, undoped semiconductor, the Fermi level is exactly halfway between the valence and conduction bands, and the valence band is completely filled, while the conduction band is completely empty. Also shown is the work function, which is defined as the energy difference from the Fermi energy to the vacuum level.

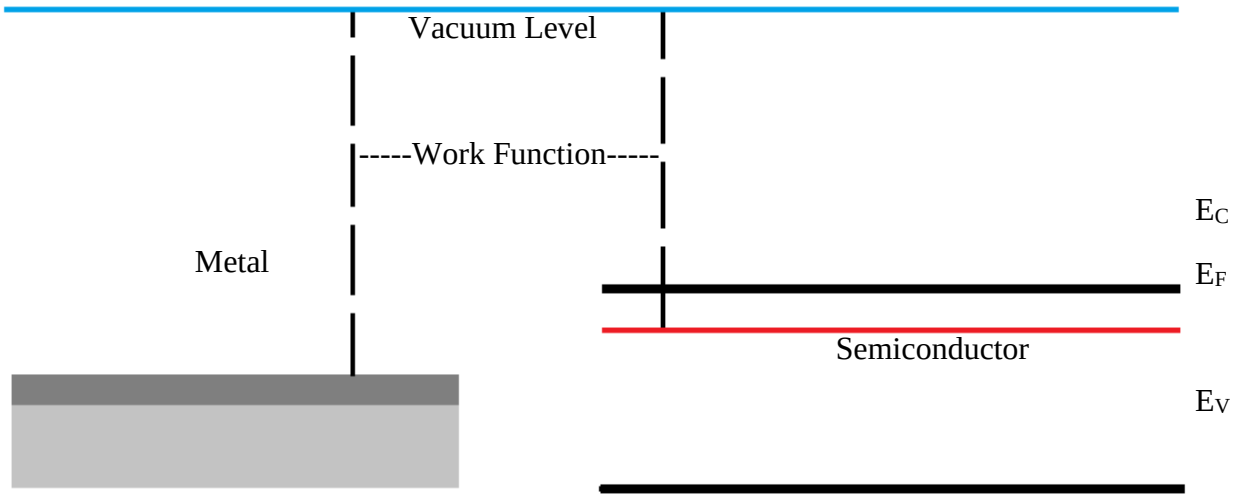

Figure 1.1. Diagram of the energy levels of a metal and semiconductor before contact is made.

Figure 1.2 shows the change that occurs to the materials' energy levels after contact is made. The Fermi levels align as the two materials achieve thermal equilibrium, and the vacuum level remains continuous, keeping a constant value away from each material's Fermi levels. In order to accommodate these changes, the valence and conduction energy bands of the semiconductor must bend. This bending of the energy levels form an energy barrier which must be overcome by the charge carriers in order to provide current to the device. If the energy barrier is a sufficiently small one, such that current flow is not greatly impeded and does not depend on

the polarity of the bias, the contact is termed an ohmic contact [1-3]. The zinc oxide photodetector device used for the research described in this paper utilized ohmic contacts.

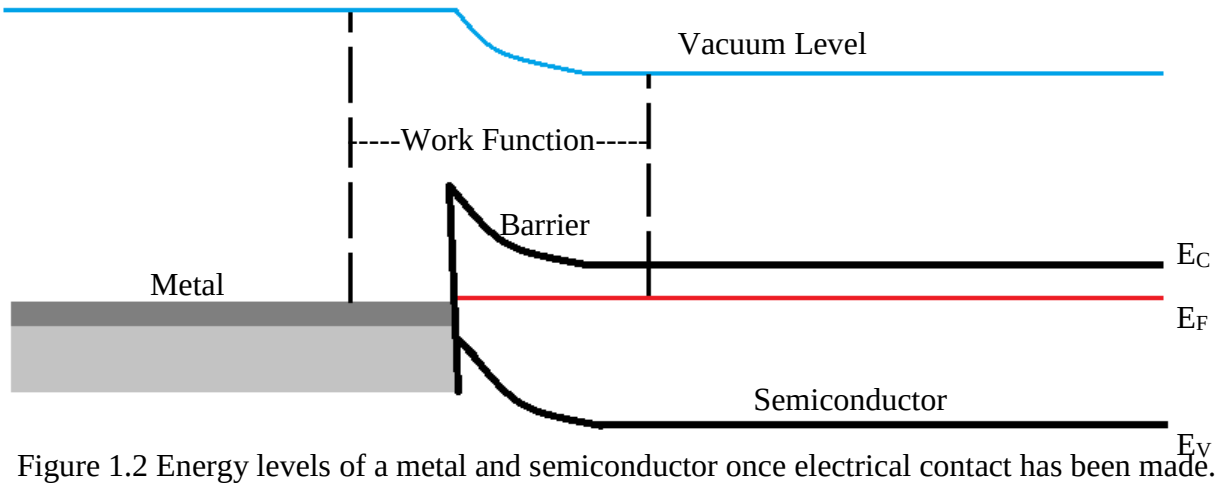

Figure 1.2 Energy levels of a metal and semiconductor once electrical contact has been made.

1.2.3. Zinc Oxide as a Semiconductor

As previously mentioned, zinc oxide is the semiconductor which was chosen for the herein described research. Initially, it was generally chosen due to the need for an ultraviolet absorber, but was specifically selected for other reasons. Mainly, those reasons were that zinc oxide is a cheap, abundant material, and also very bio safe, meaning extensive handling of it posed very little health risk. It is also a very easy substance to synthesize into nanostructures, which were needed for the photodetector device. A popular synthesis method, hydrothermal growth techniques, allows for sophisticated, quick growth which negates the possible need for expensive or complicated equipment. Finally, an outstanding quality of zinc oxide and its nanostructures, is that when grown it is quite opaque, which means light can pass through with little scattering. The applicability of this trait will become evident in a later chapter. Thus, zinc oxide was an ideal candidate for the research.

Inherently, zinc oxide is an n-type semiconductor, which means the majority of its mobile

charge carriers are electrons. It also has a large, direct energy band gap of 3.37 eV at room temperature. This width of the band gap translates into a peak absorption energy wavelength of about 355 nm (slightly variable, depending on the material morphology), which lies in the ultraviolet range [4-6]. Thus, zinc oxide is described as being an ultraviolet absorbing semiconductor, since its electrons require ultraviolet-specific radiation to jump the band gap and become mobile charge carriers. Zinc oxide's band gap is wider than many other common semiconductors, such as silicon or gallium arsenide, whose gaps are 1.12 and 1.42 eV, respectively [1]. This large band gap gives zinc oxide a high thermal stability (with a melting point of 1975 ^{o}C), meaning it can operate efficiently at higher temperatures. This property is a favorable one in the field of optoelectronics. Many of today's electronics are constructed with very densely packed integrated circuits, which must be able to maintain stable operation, despite the large amount of heat they can generate. The excess heat comes from continued scaling down of the circuits within devices which have increased power requirements and demand faster switching speeds for computational processing purposes. A semiconductor like zinc oxide is able to withstand these high temperatures and extreme environments, and thus is a promising material for current and future electronics [7-11].

Some of these useful properties, in addition to ultraviolet absorption and ability to withstand high temperatures, include piezoelectric and pyroelectric capabilities. The piezoelectric effect occurs when the gravity center of charges within certain molecules are displaced via an external force, such as material strain or compression. A separation of the positive and negative molecule charges occurs when the force is applied, and the result is the creation of an effective dipole. When this effect occurs over the entire surface of the material, it is said to be polarized, which creates an electric field able to move charges [12]. Pyroelectricity occurs in materials which are

essentially made by a large collection of smaller crystallites. These crystallites act is tiny diploes within the material. When a certain area in the crystal is heated, the crystallites become polarized. The heating, cooling, and polarization of the crystallites generates an electric field [13]. These two properties only add to zinc oxide's already long list of useful traits.

Continuing its scientific intrigue, zinc oxide also has the largest available family of nanostructure morphologies of any semiconductor. By growing in various environments and through different techniques, zinc oxide can be synthesized in the form of: nanorods, tetrapods, rings, springs, combs, ribbons, nails, quantum dots, etc. [14-19]. The shapes of the nanostructures can vary from very simple to surprisingly complex or even beautiful. Each nanostructure has its own specific properties, growth method, and usefulness, but not all possible nanostructures, properties, or applications are yet known, as new morphologies are discovered and characterized through continuing research. The specific primary zinc oxide nanostructure used for the research described in this work, was chosen due to its high surface area to volume ratio. Such a ratio was desired since high surface areas typically lead to highly active surfaces, whether that activity is a chemical or physical one. For the purposes of the research, a highly interactive light-matter-energy surface was required in order to observe and measure the phenomena to their fullest extent.

The combination of numerous nanostructures, unique properties, and ease of workability has allowed zinc oxide to be used in numerous and diverse applications. These applications range from solar cells and quantum dots to gas sensing, etc. [20-29].

1.2.4. Ultraviolet Photodetectors

Photodetectors are devices which can detect and absorb incoming light and give some indication as to the intensity of the light, based off the current generated. At their operational

heart, photodetectors utilize semiconductors with the appropriate band gap needed to absorb the desired wavelength range of light. As mentioned previously, a semiconductor will absorb a specific range of light and, through generation of mobile carriers, can produce a current in the presence of an electric field. The amount of photocurrent is proportional to the intensity of the incoming light source. Thus, it is desirable for a photodetector to have a high inherent quantum efficiency in order to perform most effectively. Quantum efficiency is defined as the percent of single output actions for each single input action. A perfectly quantum efficient photo-device would generate one electron for every photon absorbed. Photonic failure to absorb into the semiconductor can occur because of the probabilistic nature of light as well as due to surface reflection. There are two types of current in a photodetector: primary and actual. Primary is the absolute current which comes from the initial generation of charge carriers; however, this current value does not persist long. Typically, combination and annihilation of many electron-hole pairs will occur quickly, before much device current can flow. Ideally, it is desired to have as little recombination as possible in order to maintain a current-efficient device. The difference between the initial primary current and that which remains to flow after recombination is called actual current.

Photodetectors are also defined by their responsivity and response time. Responsivity refers the amount of current which is generated in a device (depending on its quantum efficiency) by a light source of a certain power rating. It is measured in photocurrent I (amps), divided by light source power P (watts/cm^2), times the device active area A (cm^2), as seen below in Equation 1.1. Peak responsivity of the device which was used for the herein described research was calculated as being .00134 A/mW, or 1.34 A/W [30].

$$R = \frac{I}{P*A} \qquad \text{(Equation 1.1)}$$

Response time is the time it takes the photocurrent of a device to go from 10 to 90 percent of its maximum value, or vice versa. This time measurement can be taken during the initial application of light upon the photodetector, or if a large intensity change occurs over a short period of time.

Photodetector gain is another important property which allows the utilization of optoelectronic devices. Gain mechanisms are those which externally or internally increase the number of charge carriers and, thus, the current in the detector. Most often, internal mechanisms of gain are utilized and can be put into three general categories: generation, transport, and amplification. Most basic is generation, where incident photons of appropriate wavelength are absorbed by a semiconducting material and an electron-hole pair are generated. This mechanism, however, does little to directly add to the current of the device. Second is transport where, via application of an electrical potential, the already available charge carriers drift in the presence of the field. The speed at which the electrons and holes move throughout the device depends on the strength of the electric field. If enough mobile charge carriers are present, the addition and strength of an electrical potential can greatly add to device current and gain. Finally, internal gain via amplification occurs in the presence of a sufficiently strong (reverse bias) electrical potential where the electrons and holes have gained enough energy to directly interact with other, non-mobile, electrons, thereby freeing them to move about the device as gained current. This is referred to as the avalanche effect, but is typically only seen in photodiode devices where the reverse bias increases the depletion layer width [30].

As a final addition to the properties of zinc oxide and the described photodetection device, it and other similar photodetectors have an additional benefit owing to their wide band gap. Since a rather large amount of energy absorption is needed to generate an electron-hole pair,

wide band gap based detectors are usually transparent to visible light, meaning they can function during the day and night.

1.3. Prior Related State of the Art Research

Much effort has been directed at discovering new methods for synthesizing previously known and unknown nanostructured materials. There are a multitude of available methods and morphologies, but some of them can be costly, difficult to reproduce, have low yields, or can require high temperatures. Thus, a secondary effort is being made to find methods for better controlling the growth parameters and products of these synthesis processes. Hydrothermal growth methods have become the ideal technique for quick, easy, and cheap nanostructure synthesis in recent years. Recently, Podloger et al. published a paper which detailed an investigation for understanding the growth mechanics of zinc oxide [31]. The paper points towards factors such as growth temperature, pressure, or pH, as well as variability in the ratios of the zinc salts and alkaline solution used for synthesis. The materials used for synthesis were zinc nitrate and sodium hydroxide, and each solution contained different molar ratios (resulting in different pH values). Two solutions were mixed and formed a precipitate which was then washed and treated to a hydrothermal reaction. For their specific set of trials, the solutions were all cooked at 100 ^{o}C, for varying amounts of time. The resulting powders were again washed, dried, and characterized.

It was found that at high pH levels, pure zinc oxide structures were formed but as the pH lowered, the precipitates also contained zinc hydroxide. Eventually at the lowest pH, only zinc hydroxide was present. The morphologies of the structures were vastly different depending on the molar ratios of the starting solutions, and further variation could be seen depending on the time of hydrothermal synthesis. Figure 1.3 shows the different structures which resulted from

differing initial solution molar ratios. This paper presented a highly analytical look into methods for controlling zinc oxide structured growth of new, unusual, and high surface area materials.

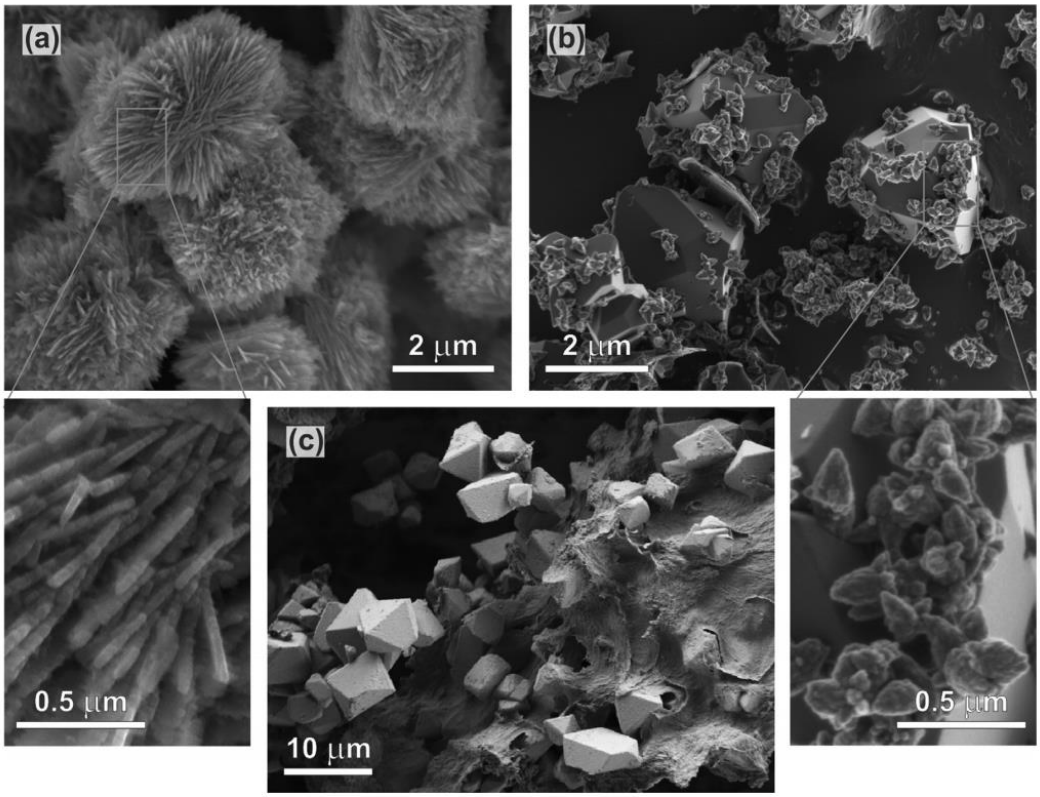

Figure 1.3 SEM images of ZnO and ZnOH nanostructures based on different hydrothermal growth times [31].

The field of nanoparticle synthesis is always seeking new, easy, and safe methods for synthesis. Lately, much attention has been focused on composite nanoparticles due to their unique properties; however, many of the previously used methods utilized hazardous material and required arduous conditions for synthesis. Azizi et al. proposed a simple methodology for green synthesis of zinc-silver core-shell antibacterial nanocomposites using wild ginger [32]. The process began with extraction of the ginger oils. After extraction, the zinc oxide silver nanocomposites were synthesized via a "one-pot" process involving the extracted ginger oils. The entire process merely required the reaction of zinc acetatedehydrate with the ginger oil and

the addition of silver nitrate, making it a simple, bio-safe, and environmentally friendly synthesis. This simple process also showed promising results as a means to synthesize materials with antimicrobial properties. In short, the zinc oxide silver nanocomposites were more bacteria-toxic as their concentrations increased and the particle size decreased. Their work represented scientific advancement in both the medical field as well as material synthesis, and has clear benefits for humanity and the environment.

In a series of systematic experiments, Bahramian et al. reported the effects of post synthesis annealing on dense, well-aligned zinc oxide nanowires [33]. Grown in a similar fashion to the research detailed in this thesis, their work described a number of properties which can be changed simply by altering the annealing temperature. Firstly, their results showed that the zinc oxide nanowire diameter increased while the distribution of diameters became more narrow with increasing annealing temperature. This can be seen in Figure 1.4.

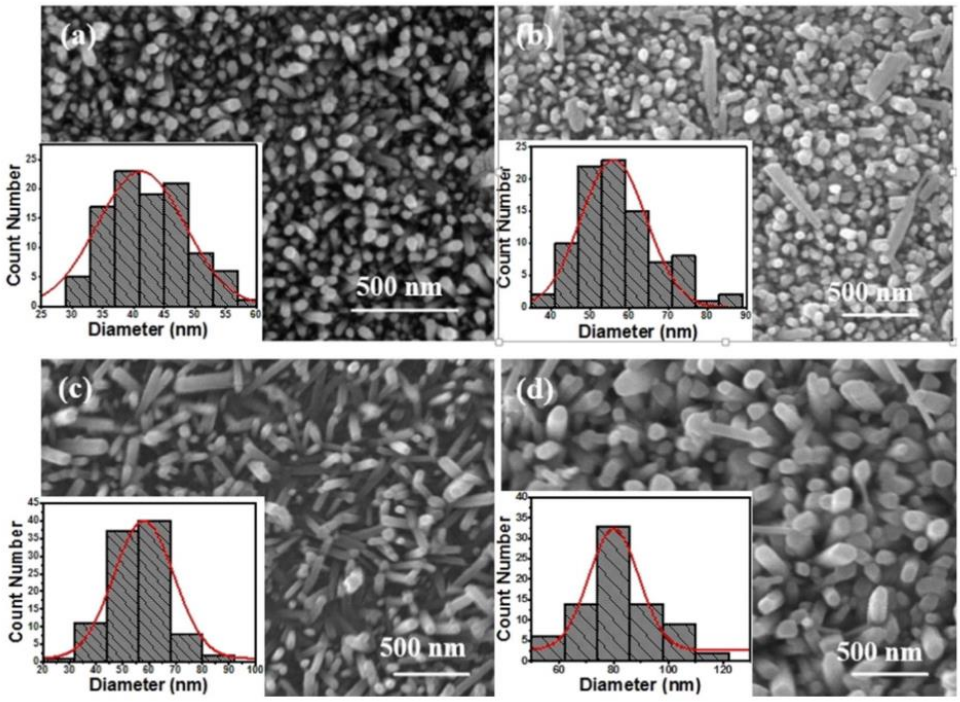

Figure 1.4 SEM images showing the effects of annealing temperature on ZnO nanorods [33].

It was also reported that a red shift away from the ultraviolet absorbance spectrum occurred as annealing temperature increased, most likely due to the increase in nanowire diameter. As expected, the nanowires were very transparent to the visible spectrum. Finally, it was shown that under no illumination and a bias voltage, the samples which were annealed at higher temperatures actually had lower photocurrents; while under ideal ultraviolet light, current increased with annealing temperatures. The results from Bahramian et al. help to shed more light on methods for growing zinc oxide nanostructures for specific applications. If nanowires of a very specific diameter or absorbance wavelength were needed for a certain experiment or device, this information would prove useful.

2. Experimental

2.1. Device Fabrication

2.1.1. Photoconductor Base Construction

The research for this thesis was conducted using a zinc oxide photodetector which was designed and constructed as follows. An opaque, single crystal, smooth cut quartz slide was cut into size. The slide was 25 mm x 10 mm x 1 mm thick. To ensure proper growth of zinc oxide on the quartz surface, the slide was thoroughly cleaned by sonicated baths in acetone, isopropanol, ethanol, and double deionized water. Each bath step took 15 minutes and the slide was allowed to dry in ambient air between steps. Once clean, the slide was topped with small copper masks along its center axis. These masks had an inverse interdigitated electrode pattern. The slide and masks were then put into a Polaron SC7620 sputter coater [34] and coated in 110 Å of gold layering. After coating, the copper masks were removed, and a gold interdigitated electrode pattern was left behind.

Before zinc oxide growth could be initiated, the gold electrodes were checked for any shorts. This was done via visual inspection of the fingers under an optical microscope. Any defects in the copper masks could be seen as a pair of touching gold electrode fingers and a separating cut was made with a micro-needle. Once the slide and pattern were inspected and cut, and the surrounding gold layer was formed into electrically separated individual electrodes, the photodetector base was completed. The gold coated slide was then baked at 350 ˚C for 0.5 hours in order to fully adhere the gold layer and ensure it did not flake off during the hydrothermal growth steps.

2.1.2. Growth of Zinc Oxide Nanostructures

Next, the primary zinc oxide rod structures were grown along the ‹001› direction, perpendicular to the similarly matched quartz crystal substrate. Sparse nanorods were hydrothermally grown using a technique similar to the process described by Zhang *et al* [35] in which equal molar ratios of 20 mM of zinc nitrate, $Zn(NO_3)_2$, and hexamethylenetetramine (HMT) were mixed into a glass vial. The slide was inserted at a specific angle into the solution-filled vial and capped off. The angle chosen was such that it facilitated optimal perpendicular growth of the zinc oxide on the slide surface. The slide and vial were put into an oven at 60 ˚C for 15 to 20 hours. After baking, the slide was slowly pulled from the vial so as not to dislocate the delicate rods, and gently washed in DDI water so any excess/loose zinc oxide particulates were removed.

The single-rod grown slide was dried in ambient air and then put in for two additional growth steps. Similar to the previous step, the two next steps included the same amounts and ratios of zinc nitrate and HMT, but had 50-100 µL of 98% diaminopropane (DAP) added into the vial. They were again heated at 60 ˚C for 2-5 hours. The DAP induced site-specific nucleation on the columnar facets of the zinc oxide primary rods. The structures which resulted had a branched nano-tree-like shape, as seen in Figure 2.1. This morphology had a very high surface area to volume ratio and nano-sized features at the branch tips. A high surface area to volume ratio typically means, any reaction observed on such structures will progress at a more rapid rate, due to the large amount of surface on which to react. It was believed the high surface area to volume ratio and small feature size of the as grown zinc oxide nanostructures played a large part in the observed experimental phenomenon, which will be later described. After hydrothermal synthesis of the nanostructures, the slides were removed from the vials, rinsed lightly, and allowed to dry in ambient air. The final step in the fabrication process was to connect the

previously isolated gold interdigitated electrode fingers in the center of the quartz slide to their respective sides of the device, using silver conductive paint. Also adhered to each side of the device electrodes, via silver paint, were small wires which would later be connected to the electrochemical workstation where a bias voltage could be applied across the device electrodes. An image of the constructed zinc oxide photodetector device is seen in Figure 2.2.

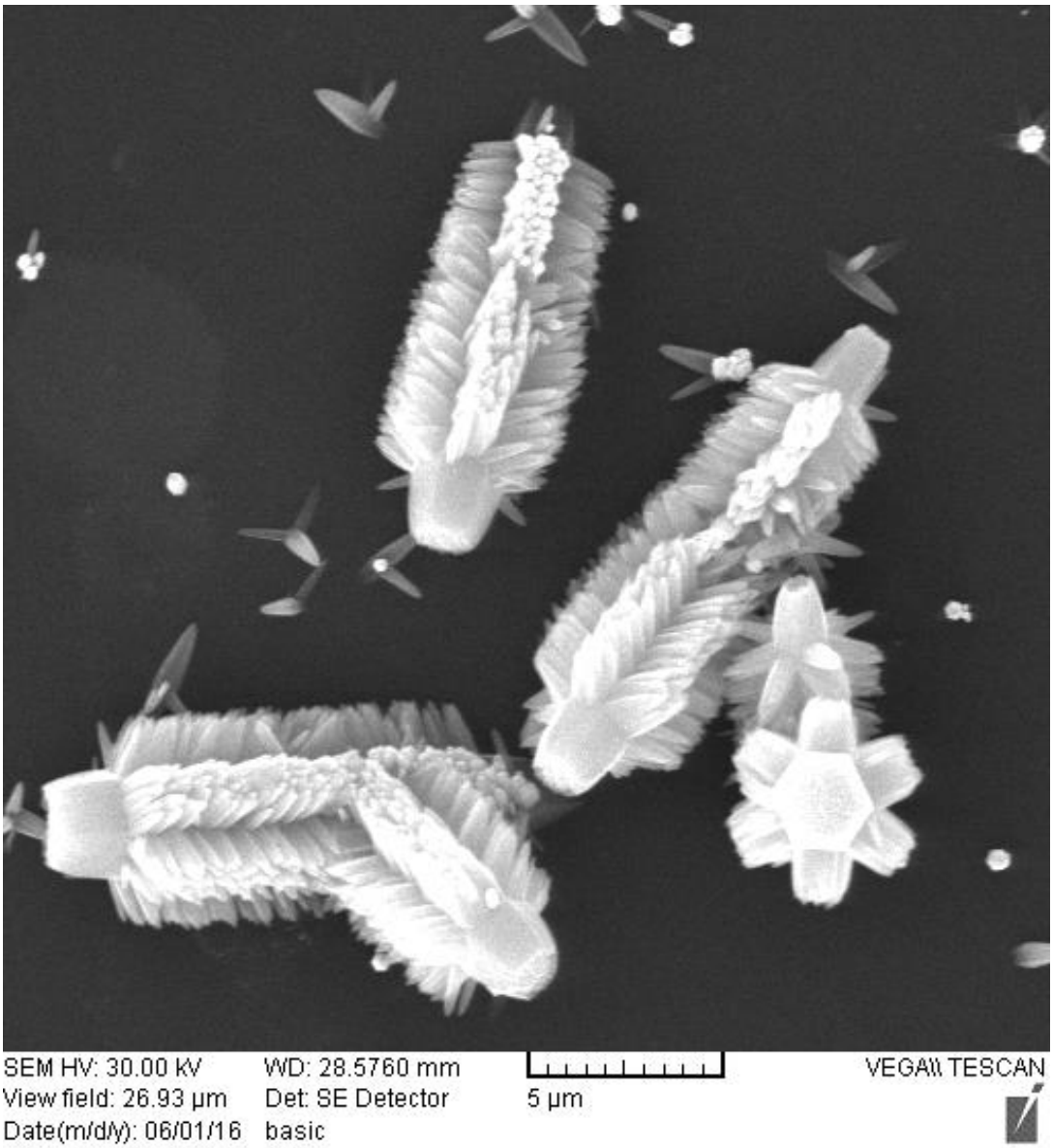

Figure 2.1 SEM image of the zinc oxide branched nanostructures.

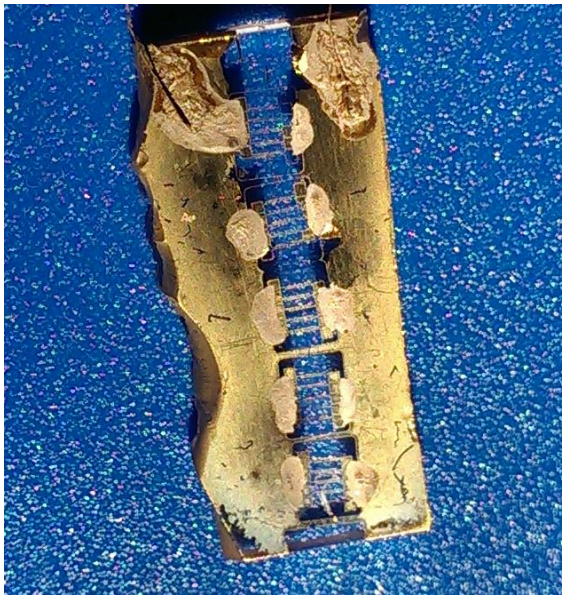

Figure 2.2. Zinc oxide photodetector

2.1.3. Experimental Assembly

With the zinc oxide photodetector constructed, the work area was set up in order to run tests on the device. The photodetector was placed into a special holder. This holder was custom 3D printed to securely hold the photodetector and aid in experimental consistency. An image of the holder and device within is shown in Figure 2.3. It had a central holding cell, wherein the device was held at various positions farther or closer to the light source, if desired. Directly behind the device was placed a simple solar cell whose purpose will be explained in a later chapter. The central cell helped shield the device from extraneous light sources and was painted black in order to minimize internal reflection. It also had two small holes at the top back of the cell which allowed wires, that connected the device and solar cell to either the electrochemical workstation or a multimeter, to exit without letting in extra light. Two cells on the side of the central one safely held magnets of various size and strength, in case magnetic field tests were performed.

The device was placed exactly 59 cm from the ABET Technologies solar-simulated light source [36], and was always kept at a constant distance in order to avoid the addition of extra

sources of error which would result from more or less light hitting the surface of the photodetector between experiments. Both the photodetector and solar cell wires exited the holder and were connected to the electrochemical workstation and multimeter, respectively. The workstation applied voltages of various ranges and patterns to the device, and the multimeter continuously measured the voltage of the solar cell.

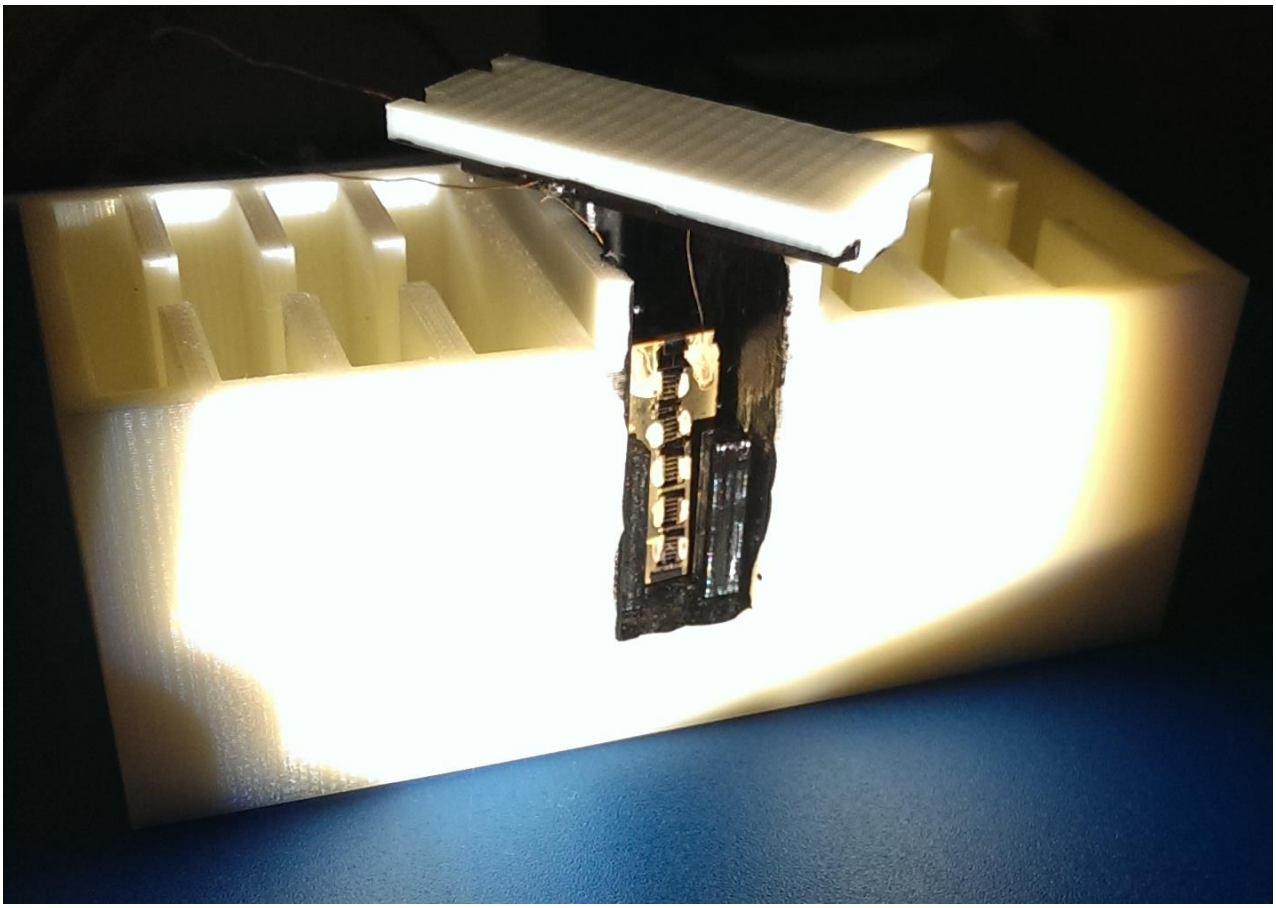

Figure 2.3. Photodetector inside the custom designed device holder.

2.2. Primary Experiments

2.2.1. Initial Applications

The base experiments which used the primary photodetector involved the device which was connected to an electrochemical workstation and a bias voltage applied across the gold

electrodes. For all of the following described experiments, unless otherwise stated, an electrical bias of 0 to 10 V, swept at a rate of 0.075 volts per second (V/s) was used. The voltage was applied in the presence of a solar simulated light source. The photons from the light source, which included the ultraviolet wavelength range, were partially absorbed by the zinc oxide nanostructures which increased the device conductivity by generating excess charge carriers and produced a measurable photocurrent. Figure 2.4 shows an ohmic current-voltage (I-V) curve of the nanostructured device under full bias.

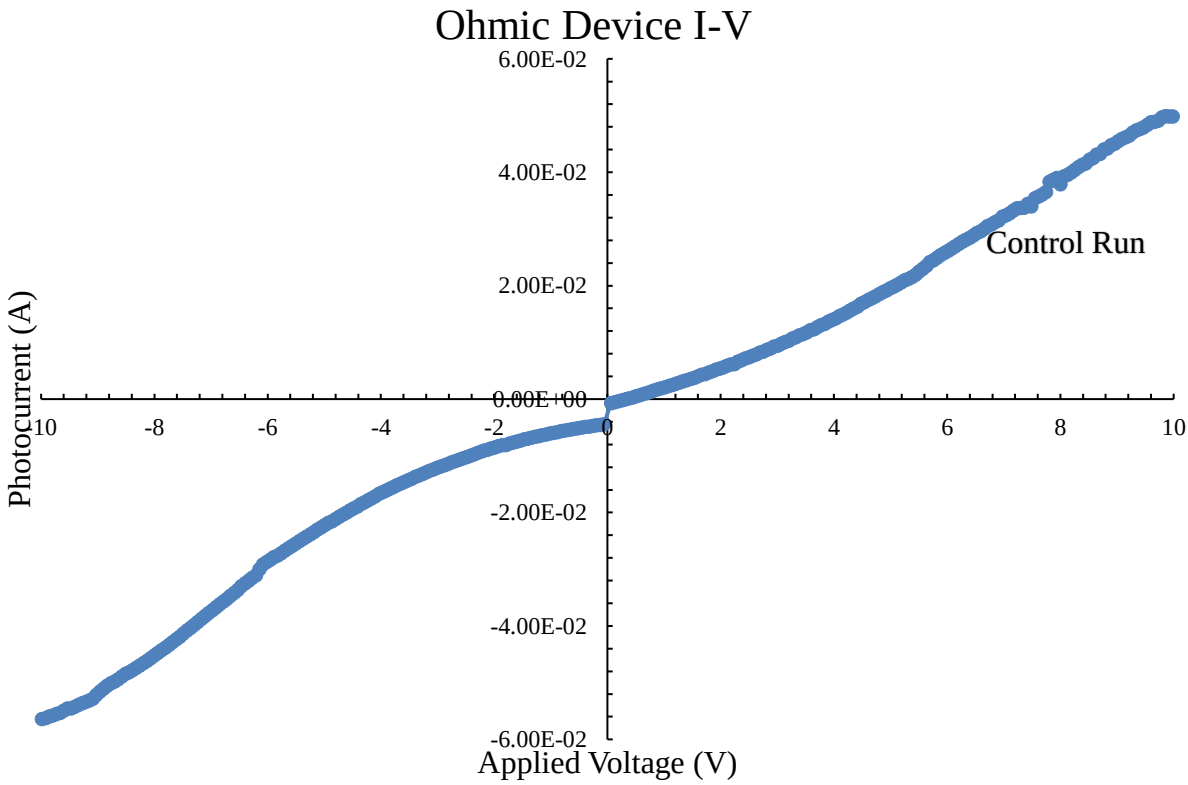

Figure 2.4. I-V curve of the zinc oxide photodetector showing its ohmic characteristics.

Once 10 V was reached, the workstation was shut off, the device experienced a zero voltage, and no photocurrent flowed through. It was obvious that the current through the device was primarily dependent on the presence of the ultraviolet wavelengths in the light source. Without the light source, the zinc oxide had fewer charge carriers and less photocurrent could flow, as

seen in the comparison graph of light and dark trials in Figure 2.5. This data was consistent with the description of semiconductor energy band theory and ultraviolet absorption described in the introduction chapter.

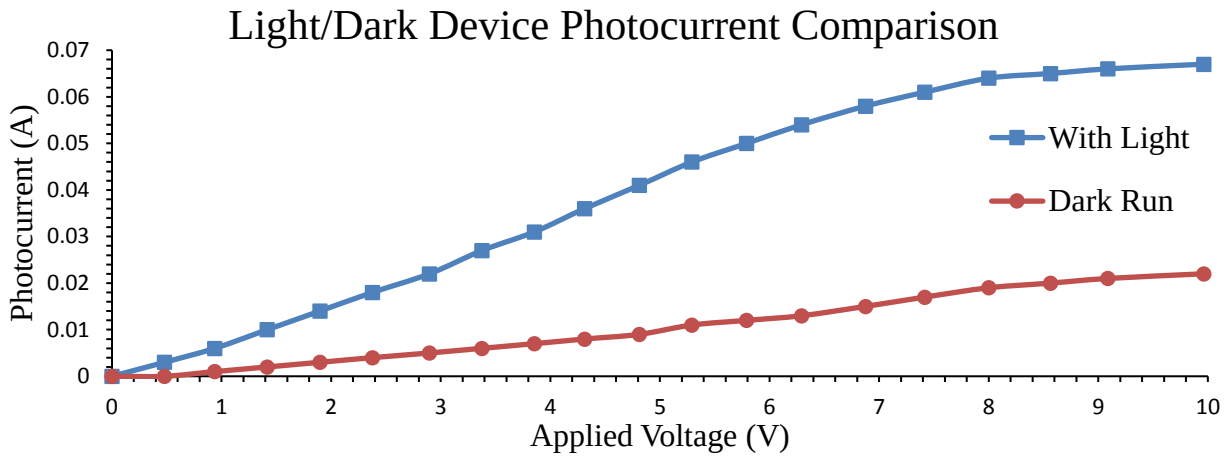

Figure 2.5. I-V curves for trials with and without the light source.

2.2.2. Basic Device Saturation

The experiments conducted showed that if after a single voltage application across the device a subsequent application was directly done, there would be an increase in the maximum photocurrent. As more consecutive applications were run, the maximum photocurrent continued to increase until, after a certain number of trials, it reached an absolute maximum. The point at which the device photocurrent would no longer increase with continued voltage applications was designated as having reached "saturation". The saturation phenomenon is shown in Figure 2.6 (top).

2.2.3. Saturation Trend

It was found that this saturation value was not an absolute maximum, but could be altered and further increased. If, after saturation had been reached, time was allowed before the next

consecutive application, an increase in photocurrent would be measured. Thus, if further time (about seven minutes) was allowed between consecutive applications, the maximum photocurrent would continue to increase to a slightly higher absolute saturation value. This final, maximum saturation value is that which will be referred to as "saturation" throughout the rest of this thesis. For the sake of efficiency and consistency, all trials mentioned hereafter were performed after this saturation value had been reached.

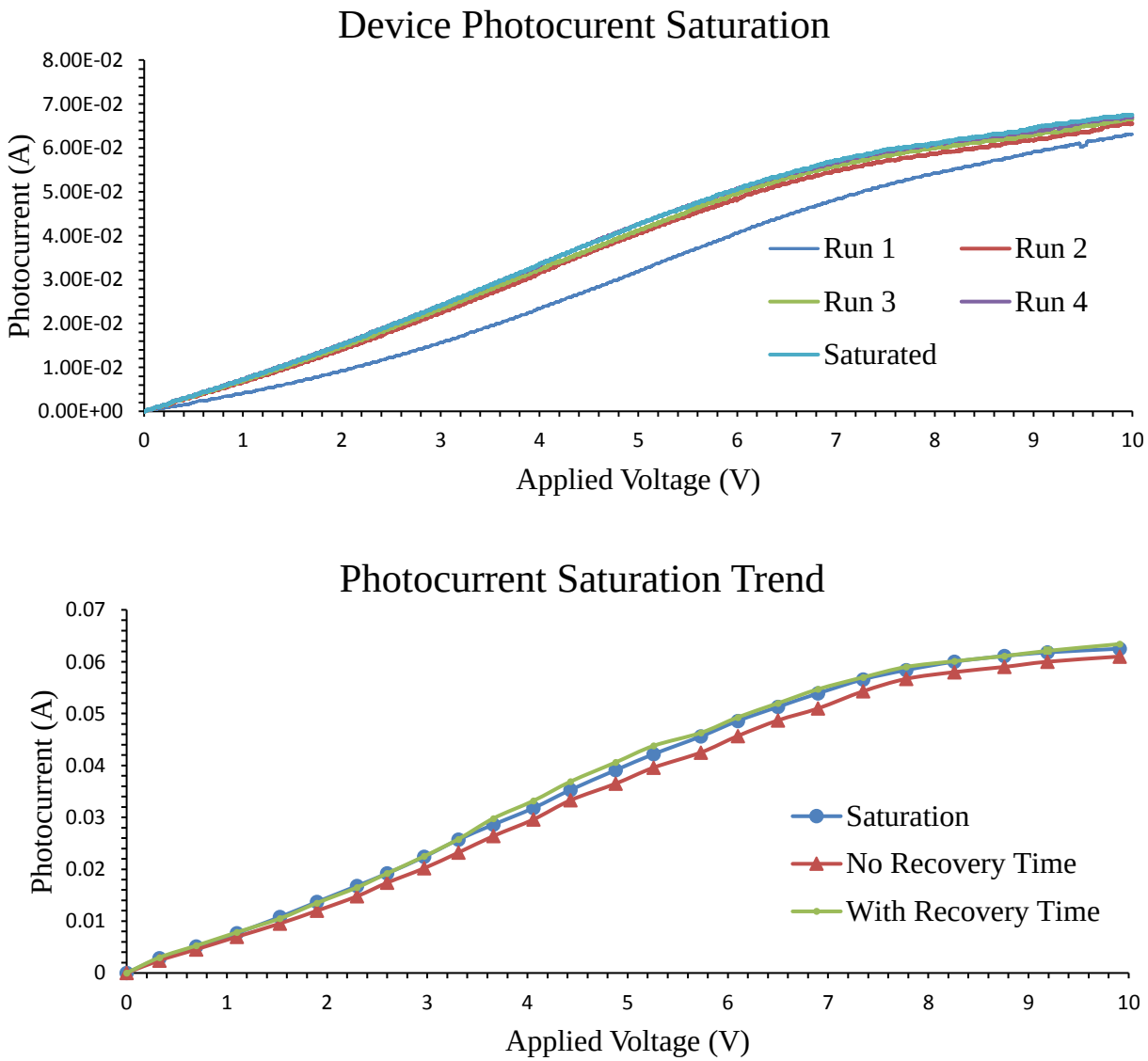

Figure 2.6. (Top) Photocurrent saturation process of the photodetector. (Bottom) Saturation trends.

A further interesting phenomenon to note is that once the final saturation value had been reached, if the next trial was run with no time between it and the previous trial, the photocurrent would be measured at a lower value than saturation. This can be seen in Figure 2.6 (bottom). The blue data line labeled "Saturation" is the top most line in the "Device Photocurrent Saturation" graph. The preceding voltage application was done with no time after the first and is labeled as "No Recovery Time". The photocurrent of this trial was about 4% less than the previous trial, and yet the only experimental variable was the time between voltage applications. The next trial, labeled "With Recovery Time", proceeded with ample time (about seven minutes) after the previous trial, and it can be seen that the photocurrent increased back to the saturated value.

These initial results posed many questions and set the stage for further experimentation. A further investigation into the previously mentioned, and other observed, phenomena was initiated in an attempt to identify new properties and characteristics of these nanostructures. Thus, the following trials represent various systematic experiments which methodically subjected the photodetector device to different conditions in order to measure their effect on the device and its properties.

2.2.4. Ultraviolet Filter

This experiment involved using an "Omega Optical" optical filter [37] which allowed only light wavelengths less than 410 nm to transmit. The filter was placed directly at the opening of the holder such that any light reaching the device inside must first be filtered. Since zinc oxide is a known ultraviolet radiation absorber, this trial acted as a test to ensure that the nanostructures were not being affected by any other range of wavelengths from the solar simulator. Figure 2.7 shows the photocurrent of a controlled voltage application as well as one in which only filtered,

ultraviolet light was incident upon the device surface. It can be seen that the filter had almost no effect on the photocurrent, as expected. The active range of ultraviolet radiation was not affected by the filter and, thus, there was no change in the conductivity on the zinc oxide.

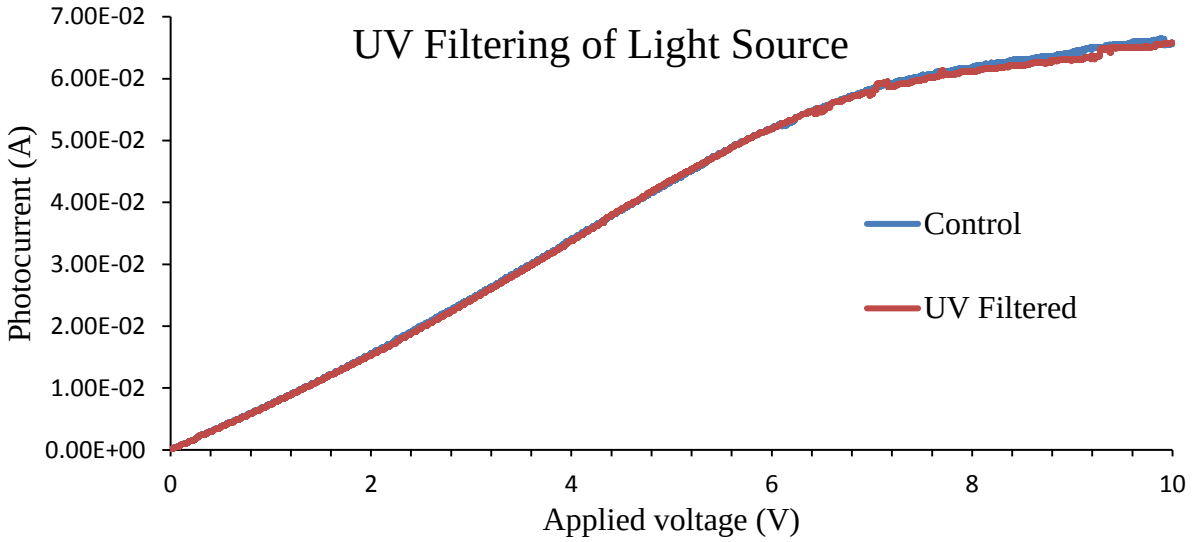

Figure 2.7. I-V curves for a control and ultraviolet radiation only trial.

2.2.5. Increased Intensity

The next experiment required the light source to be focused which increased its intensity and caused more photons per area to be incident on the device surface. This was a test trial to confirm that the device followed known principles. In this case, it was if the photonic density of the incident light was increased, then the conductivity and photocurrent should also increase. Figure 2.8 shows a graph of a control data set and one in which the light source intensity was focused from a diameter of 10 cm down to 6 cm. The difference in area which resulted from this focusing was 36%. If there had been more ultraviolet light per area on the device face absorbed by the zinc oxide, then it should have generated more carriers which would have resulted in a higher photocurrent; that is what was observed. Thus, to the extent of reaction to variable light intensities, the nanostructures and device operated in a predictable manner.

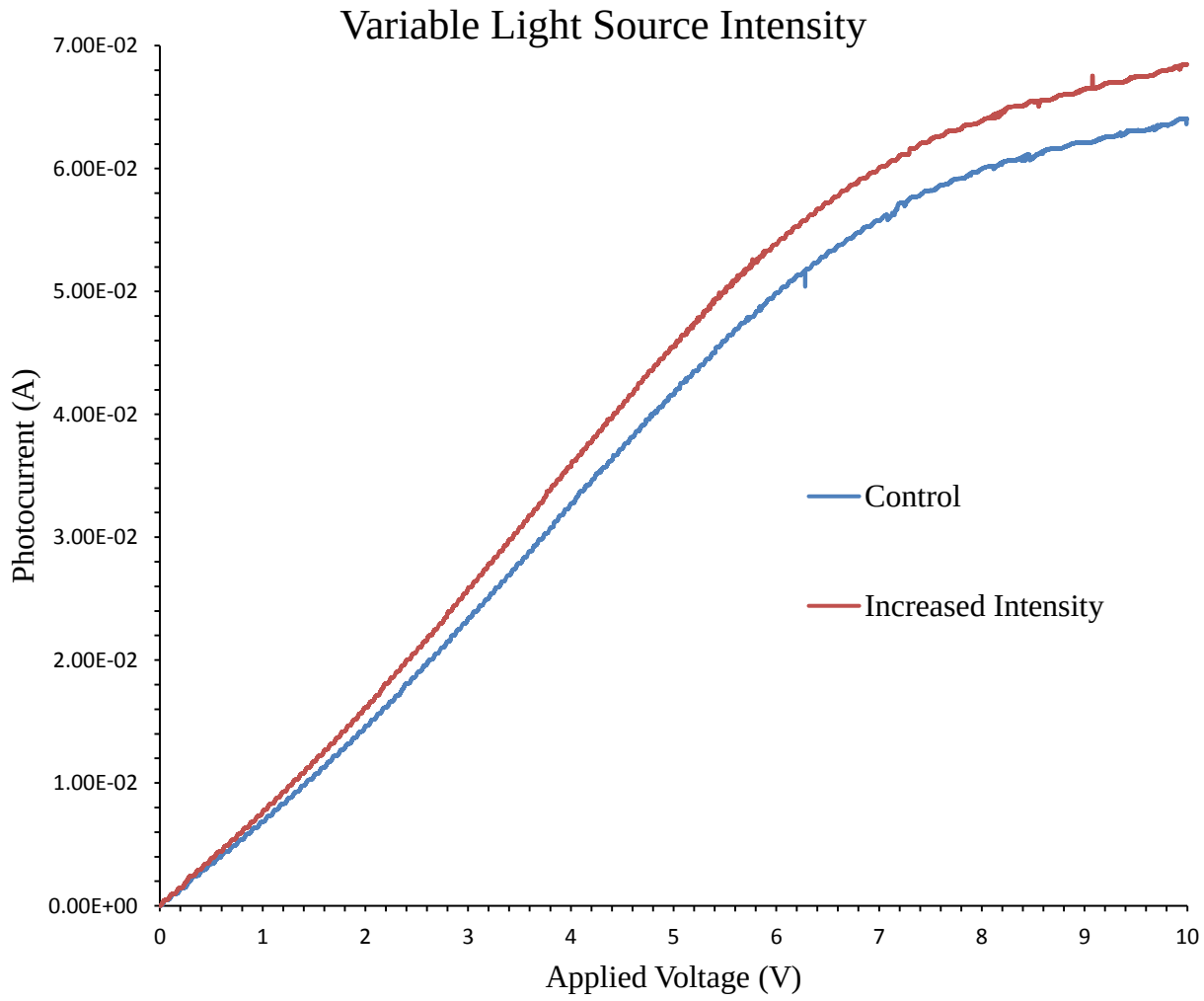

Figure 2.8. I-V curves for a control and focused light source trial.

2.2.6. Variable Atmosphere

One hypothesis which could possibly shed light on the variable photocurrent phenomena involved surface oxidation of the zinc oxide. Therefore, voltage sweeps were applied to the device in different atmospheres and changes in photocurrent were measured. In those trials, the device experiments were performed in ambient air atmosphere as a control, in an oxygen-rich atmosphere, and in an oxygen deficient atmosphere with the use of argon. Figure 2.9 shows the photocurrent measurements of those trials. The implications of this data will be discussed in a later chapter.

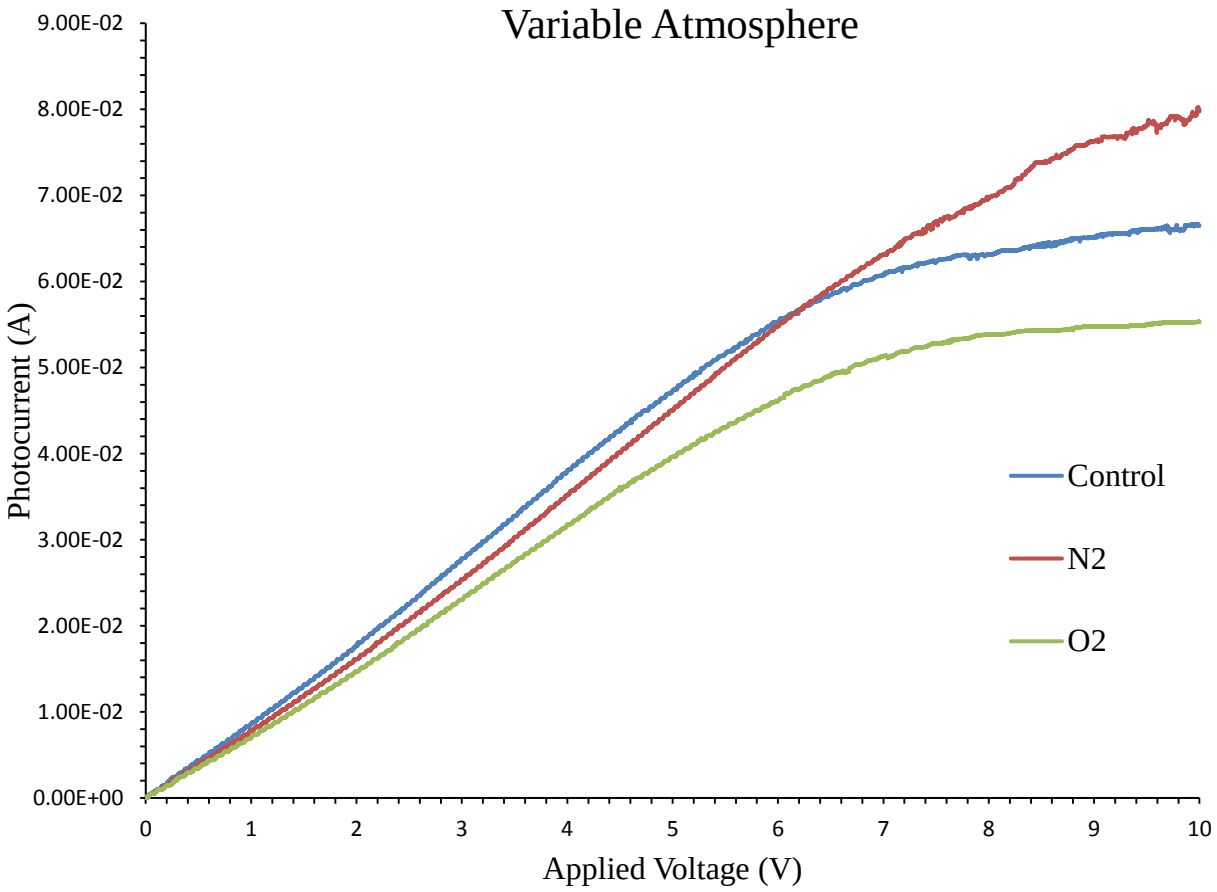

Figure 2.9. I-V curves of trials under ambient, nitrogen, and pure oxygen atmospheres.

2.2.7. Sweep Rates

As part of a thorough experimental process, the device was run through voltage applications of varying sweep rates. The separate applications were run at rates from 0.065 V/s to 0.2 V/s and the photocurrent measurements of those trials are shown in Figure 2.10. As per standard, all trials were run after device saturation had been reached. The figure shows that the photocurrent through the device varied slightly between the different sweep rates, with 0.2 V/s having the highest maximum measured current. The implications from this data, however, have yet to be fully understood. One possible explanation for the sweep rate dependent current could be related to the response of the device in reaction to the variability of charge speeds.

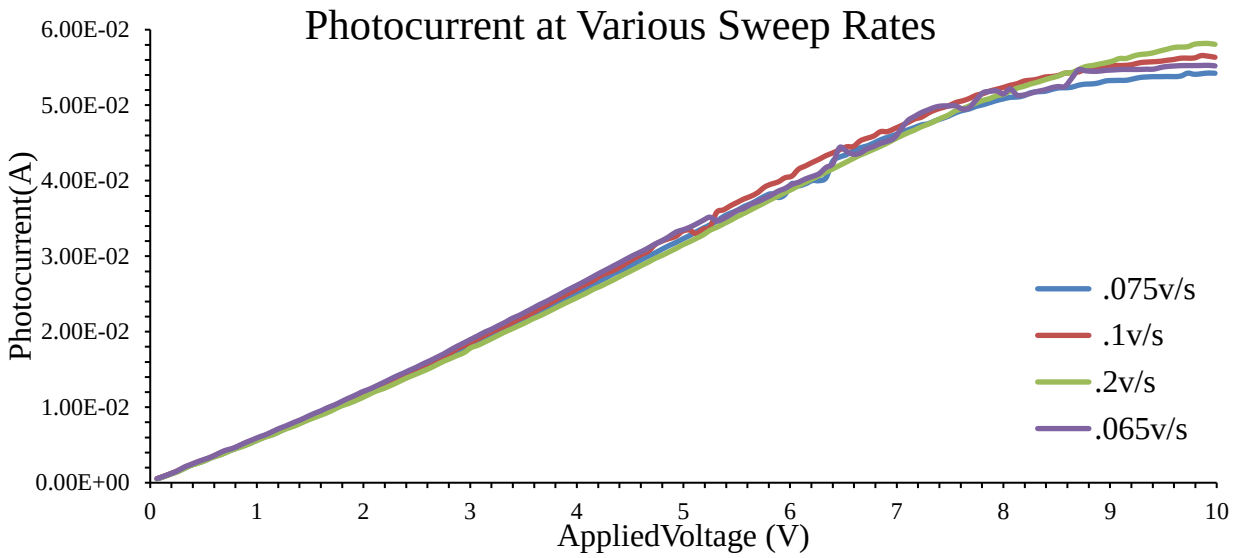

Figure 2.10. I-V curves of the photodetector under different voltage sweep rates.

2.2.8. Device Temperature Measurements

Finally, the last set of experiments presented in this section involved measuring the surface temperature of the device during voltage application. For the same reason as running variable sweep rate experiments, it was necessary to gather as much data about the device as possible in order to have a complete understanding of its properties. Device saturation was carried out as room temperature argon was blown across the surface of the photodetector. Once saturation was reached, the following two trials were run with the argon supply hose submerged in liquid nitrogen. The super-cooled liquid nitrogen quickly and effectively chilled the hose and argon within. The chilled argon was then blown onto the surface of the device with the intent of cooling its surface. An infrared hand-held temperature measuring device was used during trial sweeps. The temperature sensor was held close to the device surface, without blocking any light from the solar simulator, and temperature measurements were taken every ten seconds. Figure 2.11 shows those temperature measurements. The values in the figure are normalized to their starting values so that each initial temperature measurements started at one. Thus, for the point

from the “Cooled” trial at 130 seconds, 1.14 represents a temperature approximately 14 percent higher than its starting value.

This experiment presented some issues in regard to data measurements. Primarily, the hand-held temperature device measuring infrared beam was invisible to the naked eye and, while there was a visible guiding laser beam, the distance between the two was great enough that it caused inconsistencies in keeping the actual measurement beam in the same spot during and between trials. The measuring device had to be held very still in order to read temperature from the same spot on the photodetector, but this proved difficult with the small, invisible measuring beam and small photodetector surface. Ideally, only temperature measurements of the small zinc oxide active area would be taken, but any slight shake, such as from pulling the measuring instrument’s trigger, moved the measuring beam off course.

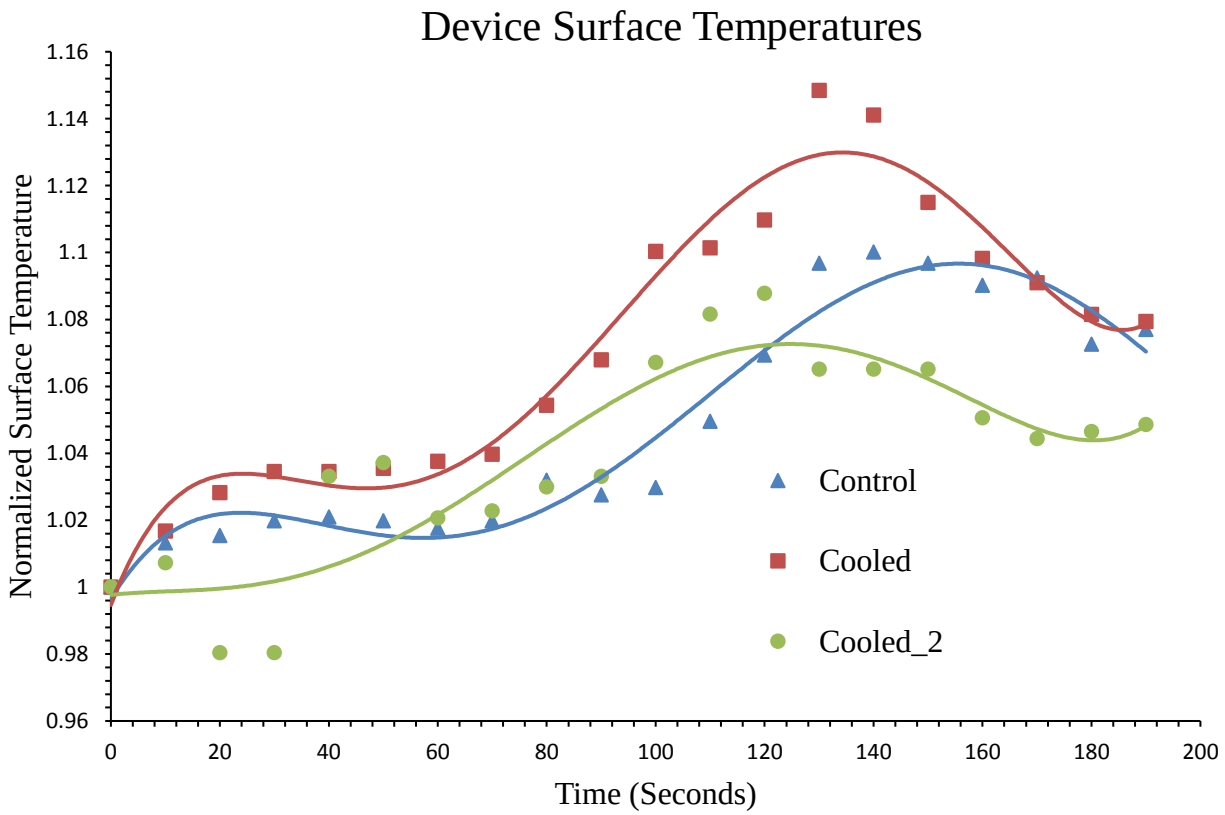

Figure 2.11. Approximate surface temperatures of the photodetector during voltage application.

The data from Figure 2.11 does appear to be somewhat askew, since the trial labeled "Cooled_2" was run under the same conditions as "Cooled" but shows a much greater increase in temperature. Also, the "Cooled_2" trial indicated that in the presence of flowing, chilled argon, the temperature of the device rose even more, which contradicts the logic that a colder flowing gas should cool the surface of the device. Nevertheless, there can be seen a general trend that the surface temperature increased during voltage application, with maximums approximately near the end of the sweep (135 seconds), followed by cooling of the device after voltage application. More controlled, accurate experimental conditions and equipment would be needed to validate the data in Figure 2.11.

2.3. Secondary Experiments

2.3.1. Addition of Solar Cell

The second major facet of this research was centered around the light transmitted through the photodetector during voltage application. It was hypothesized that by measuring the amount of light transmitted through the device, insight into the cause of the variations in photocurrent could be gained. Any additional data gathered about the variable photocurrent could have proved useful. Therefore, simple four-operation calculators were acquired from which the solar cell was removed and inserted directly in contact with the back of the quartz substrate of the photodetector. Figure 2.12 shows a cartoon representation of a side view the device and solar cell attached. A multimeter was attached to the solar cell in order to measure the voltage during application of bias across the device. The initial hypothesis was that some small fluctuations in cell voltage during application might have been measured, but what was observed was entirely different and posed its own myriad questions.

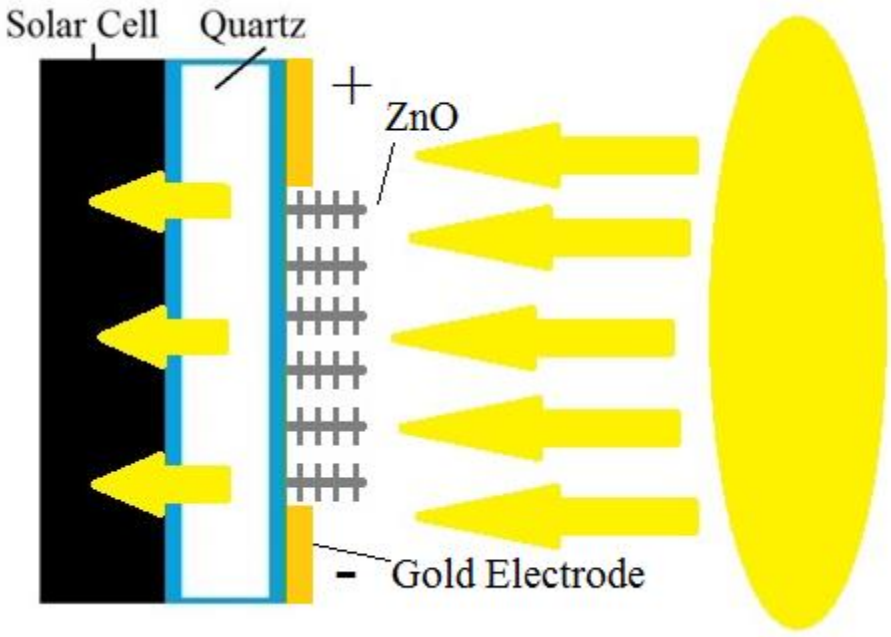

Figure 2.12. Side view representation of the contact between the photodetector and solar cell.

2.3.2. Control Trial Cell Measurements

The data measurements of the solar cell during a standard voltage application of 0 to 10 V at 0.075 V/s showed that the voltage of the cell drastically decreased at higher voltages. Something was actively interfering with the photons as they interacted with the photodetector, passed through the quartz substrate, and reached the solar cell. The photons were either being blocked, scattered, or absorbed by some mechanism. Figure 2.13 shows the normalized solar cell voltage (blue) during voltage application from 0 to 10 V (red).

It could be seen that the cell voltage decreased with an increase in bias across the device, eventually reached a minimum, and then slowly returned close to, or at the prior maximum value. Most interesting, however, was the small amount of time which elapsed between the voltage application stop time (denoted by the dashed red line) and the actual minimum of the cell voltage. This phenomenon, which was termed “lag time”, was always present during standard voltage applications, but what the cause of the effect was unknown.

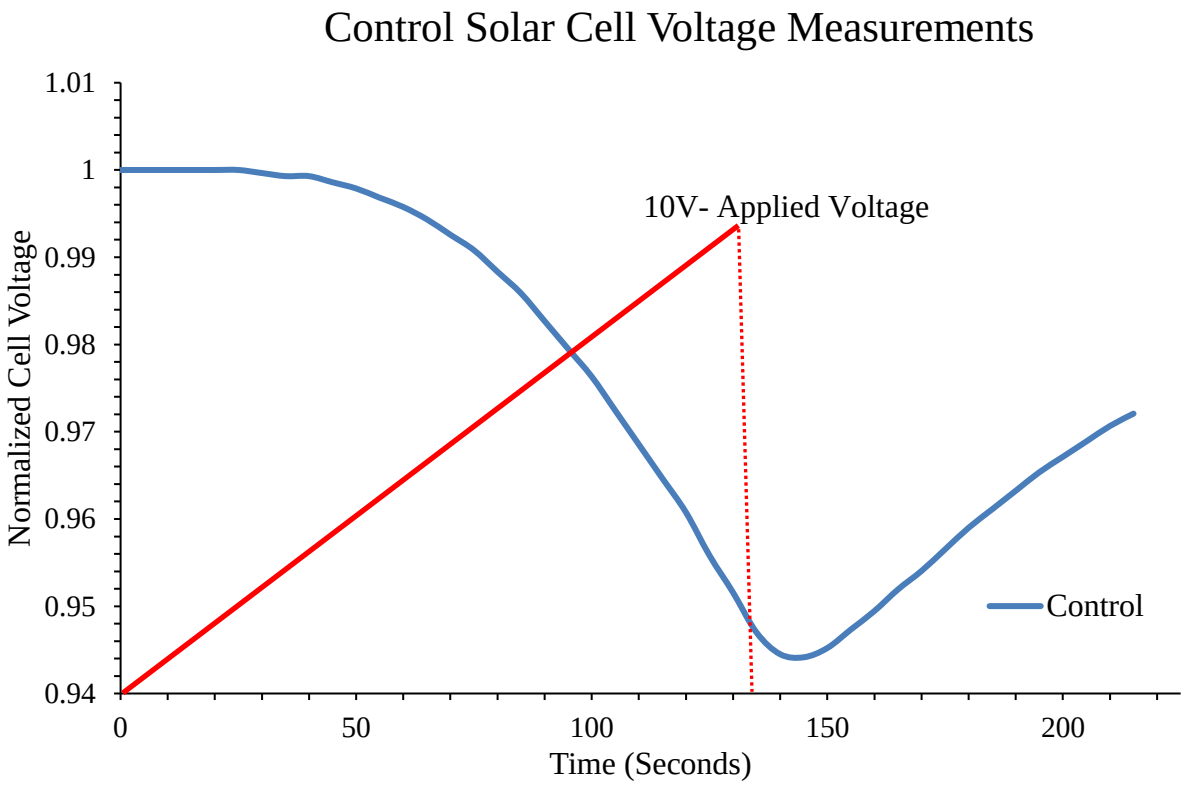

Figure 2.13. Normalized solar cell measurements (blue) as a function of applied voltage (red).

Nonetheless, the data showed that whatever mechanism was acting to interfere with transmitting photons, it was initiated by the voltage application but was not entirely dependent on the voltage to temporarily maintain the effect. This was evident because the solar cell voltage drop continued even after the applied voltage was stopped and reached an immediate value of 0 V. During lag time, the voltage of the solar cell continued to decrease without any applied device voltage until it eventually leveled off and began to rise again. This meant that whatever interfered with the light continued in effect and increased for a short while after the applied voltage was removed. The data also indicated that this light-interfering effect persisted and took some time to dissipate, as seen by the slow recovery to the initial maximum value. It was because of this characteristic solar cell voltage recovery, that the time between device voltage applications was called recovery time -the time required for the cell voltage to return to its prior

steady state value before another voltage sweep was applied. In all trials, recovery time was allowed between applications unless specifically stated otherwise.

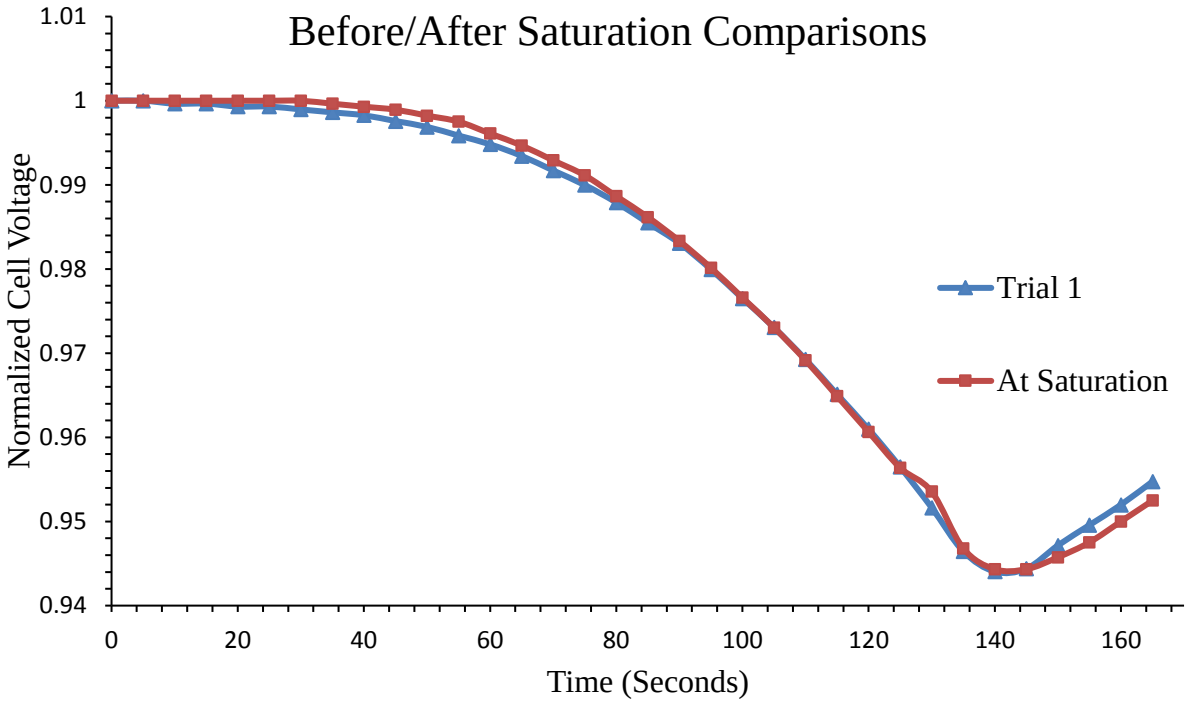

Figure 2.14. Solar cell voltage comparison of first and "saturation" trials.

This new data added to the long list of questions about the photodetector, zinc oxide nanostructures, and their properties. It was hypothesized that perhaps the photonic interference was a result of the charges generated by the absorbed incident light and moved by the applied voltage. This seemed plausible as a higher voltage produced a stronger electric field between the device electrodes, which sped up the electrons, produced more photocurrent, and could have blocked more light. Perhaps these electrons were "bumping" into the photons and scattering them. In order to determine if this explanation had merit, solar cell measurements were compared between the first trial application and a trial at saturation. The two trials had very different photocurrent measurements, and if any effect on the transmitting photons had been due

to the moving charges, this comparison would have shown the evidence. Figure 2.14 shows the normalized cell voltages of an initial "trial 1" and a trial at photocurrent saturation. The graph shows that there was very little difference between the two voltage measurements, thus the observed changes in solar cell voltage were not directly affected by the device photocurrent.

2.3.3. Solar Cell Under Ultraviolet Filter

Continuing from the previous section where an ultraviolet filter was added to the solar simulated light source, Figure 2.15 shows normalized cell voltages during device voltage application under controlled and filtered conditions. The control trial is in blue and UV filtered trials are in green and red. "With UV Filter_2" was run in order to confirm consistency in the change in cell voltage. The data indicated the trials which involved the ultraviolet filter produced a greater decrease in the measured solar cell voltage.

Obviously, with the filter in place, a lesser overall number of photons were incident upon the device surface and, thus, the cell voltage should be lower. Keep in mind, however, that these graphs display a normalized voltage value, and what is really shown is a relative percentage of the total number of photons transmitted through the device and picked up by the solar cell. Thus, a similar decrease in the relative percentage of light which reached the solar cell, between one trial (ex. Control) and another (ex. With UV Filter), would be represented by two very similar lines of data; however, this was not the case in the graph below. The data in this graph seemed to indicate an importance in the wavelength of light which interacted with the device. It is known from a previous section that the ultraviolet filtered light has no effect on the photocurrent since zinc oxide only absorbs ultraviolet radiation; however, the ultraviolet light seemed to be more susceptible to the light-interfering phenomenon which produced the decrease in cell voltage during device voltage application.

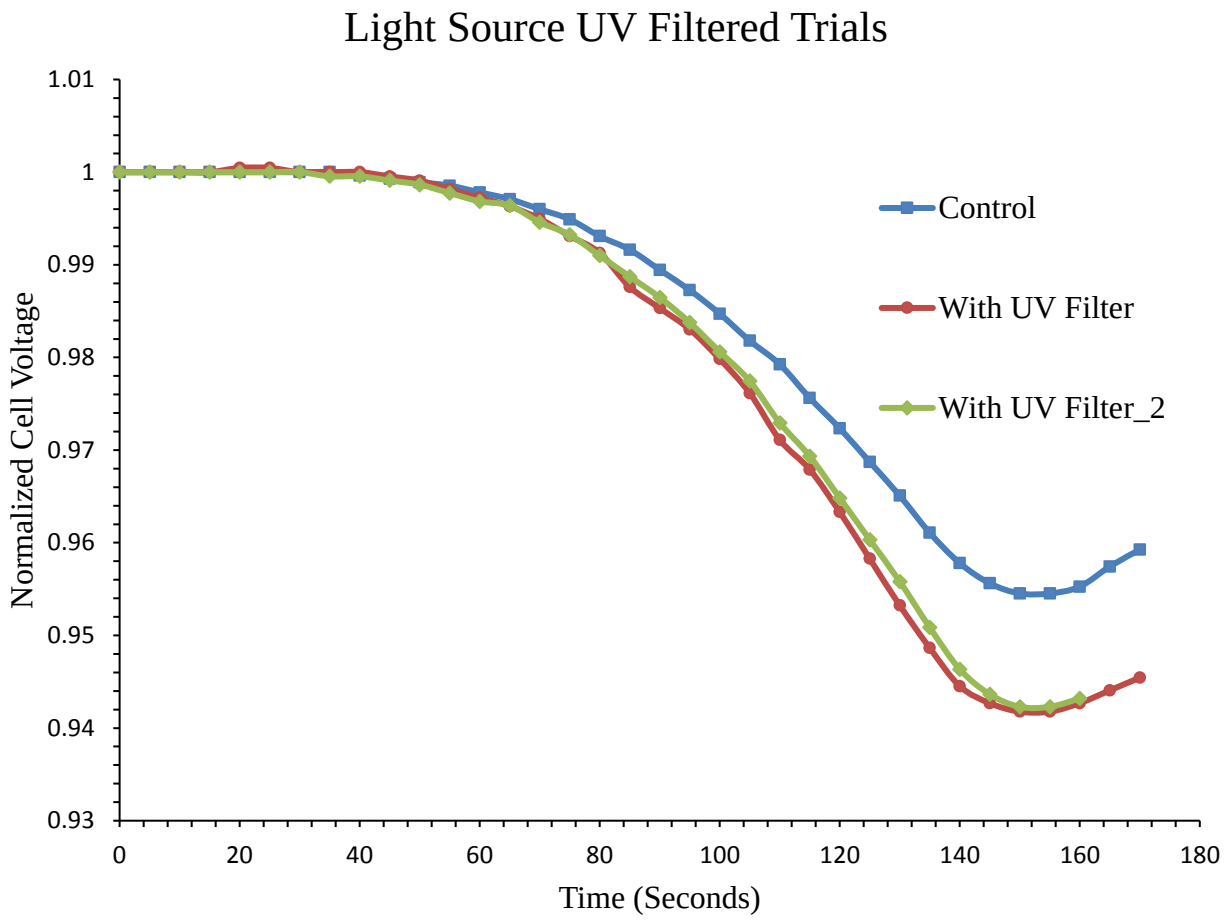

Figure 2.15. Solar cell voltages of control and ultraviolet only trials.

2.3.4. Solar Cell in Variable Atmosphere

Normalized solar cell voltage measurements can be seen in Figure 2.16. Similar to the previous section, in this experiment the device was surrounded by either air or an inert atmosphere, argon (Ar) in this case. Figure 2.9 showed that the photocurrent was higher for the trial in the inert atmosphere, N_2, and Figure 2.16 below shows that the argon submerged solar cell voltage decreased to a lower minimum during the voltage sweep than the control did. Again, it was seen that changing a single variable (atmosphere) in the experiment, resulted in a change in the number of photons which transmitted through the device. Further explanation and hypotheses will be detailed in the results chapter.

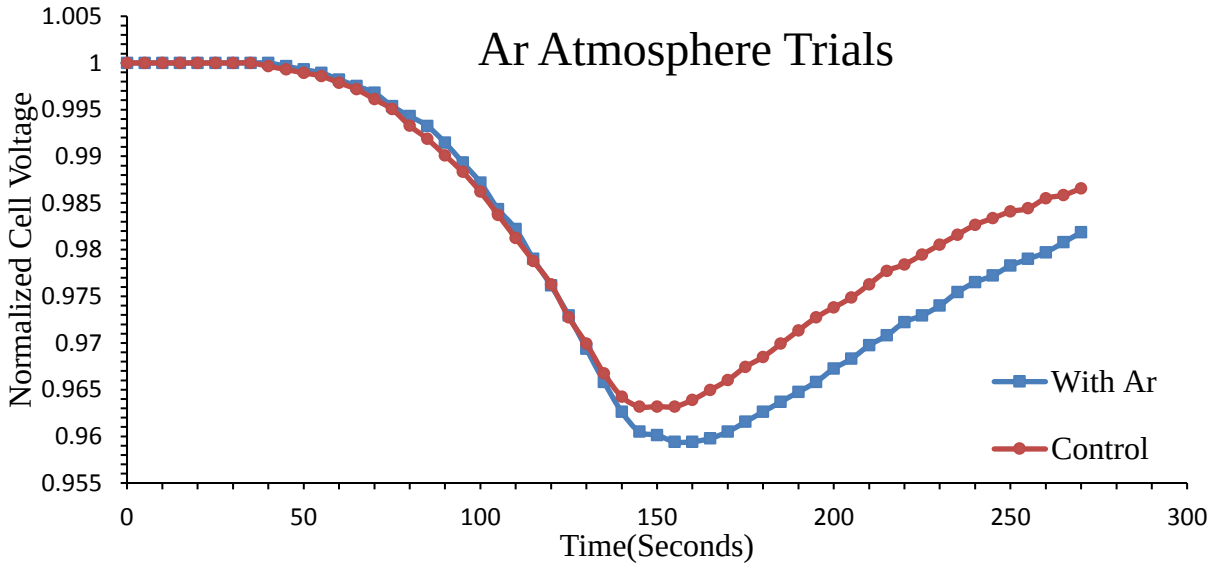

Figure 2.16. Solar cell voltages of control and argon atmosphere trials.

2.3.5. Solar Cell with Increased Intensity

The normalized solar cell voltage measurements for the increased light source intensity trial are shown in Figure 2.17. Photocurrent measurements of the increased intensity runs showed an increase in the maximum current, which was expected as the higher photonic density generated more charge carriers in the zinc oxide. As similarly explained, a more focused light source does produce a higher solar cell voltage, but since a normalized voltage is shown, as long as the approximate percentage of photons which transmitted past the device and onto the cell during bias application was the same, the graphs between trials should also look the same. In fact, it could easily be hypothesized that if incident photonic density was increased, a higher, or close-to-control percentage, should have been picked up by the solar cell. However, Figure 2.17 shows a seemingly logic-contradicting outcome. The approximate percentage of the now more dense photons which transmitted past the device and into the solar cell was actually less than that of the control run. This data represents a very surprising result of the experiment where the only new variable was not a change in the light itself, the device, or surrounding environment, but

rather a change in the amount of light. This increase in incident light density also increased the effect of the light-interfering mechanism.

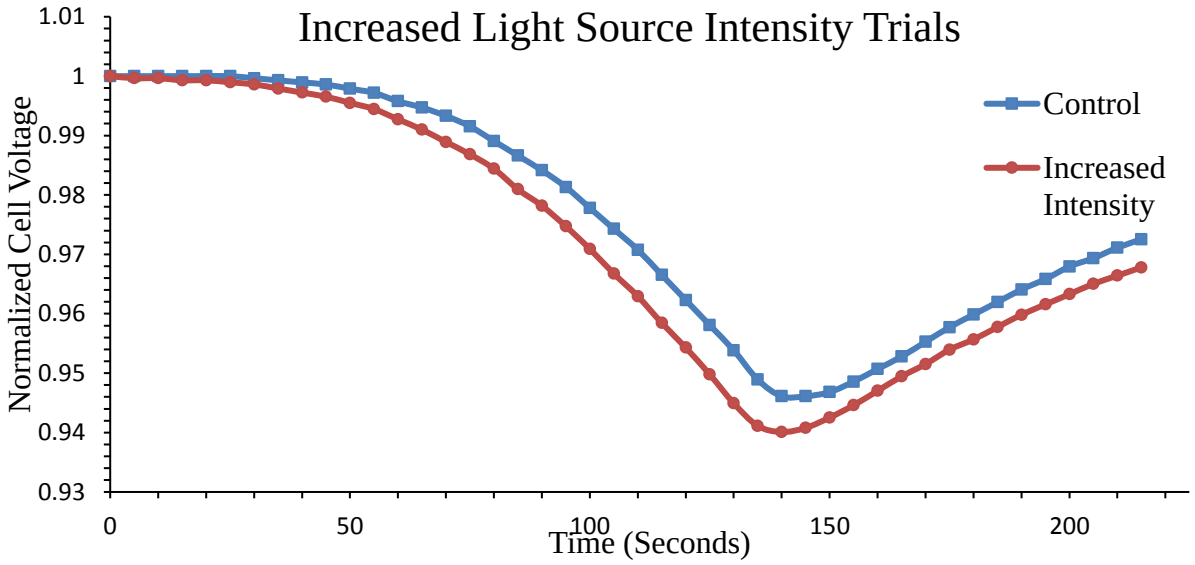

Figure 2.17. Solar cell voltages of control and focused light source trials.

2.3.6. Ultraviolet Filter and Argon Atmosphere Combined

Possibly the two most important sets of trials in terms of information provided from the data were the ultraviolet and variable atmosphere trials. The zinc oxide nanostructures were sensitive to ultraviolet radiation and responded primarily to this stimulus. Since it was believed that the phenomena observed were unique to these specific nanostructures, one could conclude that there also existed some direct or indirect relationship between the zinc oxide-specific ultraviolet radiation and those phenomena. Also very important was the previously explained variable atmosphere trials; the data gathered from those trials helped to explain the overall cause of the variability in photocurrent during voltage application. Changing oxidation levels in the zinc oxide nanostructures clearly caused a significant change in the measured photocurrent, and also gave rise to differing photonic transmission through the device. Using the UV filter had no effect on the photocurrent, as expected, but did result in less light reaching the cell during the

bias sweep. However, during voltage application in an inert atmosphere, there was a noticeable difference in photocurrent as well as a change in the transmission of photons.

Thus, it was necessary to perform an experiment with the two variables simultaneously in place so the combined effects they may have had on photocurrent and photonic transmission could be observed. Figure 2.18 shows the photocurrent measurements (Top) and normalized solar cell data (Bottom) from a trial in which the photodetector was placed in a box with an argon rich environment. The box let in the typical amount of light, but in the case of this experiment, also had all non-ultraviolet incident light filtered out as in a previous experiment. These conditions were present during the initial saturation phase as seen from "Sweep One" to "At Saturation" in the photocurrent vs. applied voltage graph below. Once saturation was reached and a final solar cell measurement was recorded, the ultraviolet filter was removed during the recovery of the solar cell voltage. Once recovered, another voltage application called "No UV Filter" was run. Afterwards, during solar cell recovery, the argon atmosphere was flushed and replaced with ambient atmosphere. The final trial which was run is labeled as "No UV Filter or Ar" and should represent standard saturated conditions. The normalized cell voltage graph in Figure 2.18 (Bottom), shows the cell voltage measurements starting at device saturation.

The data gathered from this experiment gave results which complied with and reinforced previous related experiments. The saturation process proceeded as normal, where the photocurrent incrementally increased with consecutive voltage applications and ample recovery time between trials. A saturation value was reached, followed by an identical photocurrent measurement in an additional, confirming sweep. After the confirming sweep was run, the following trial had the ultraviolet filter removed directly after the previous trial application. It

was at this point that an additional increase in photocurrent can be seen in Figure 2.18 (Top). Previously noted in Figure 2.7, the addition of the ultraviolet filter had no effect on photocurrent. A plausible reason for the photocurrent increase seen in this experiment was the excess solar simulated light incident on the box which contained the sample, sample holder, and argon atmosphere. This excess light, fully incident on the testing apparatus, likely heated the equipment and atmosphere around it, including the photodetector, which thermally generated more charge carriers resulting in a higher photocurrent.

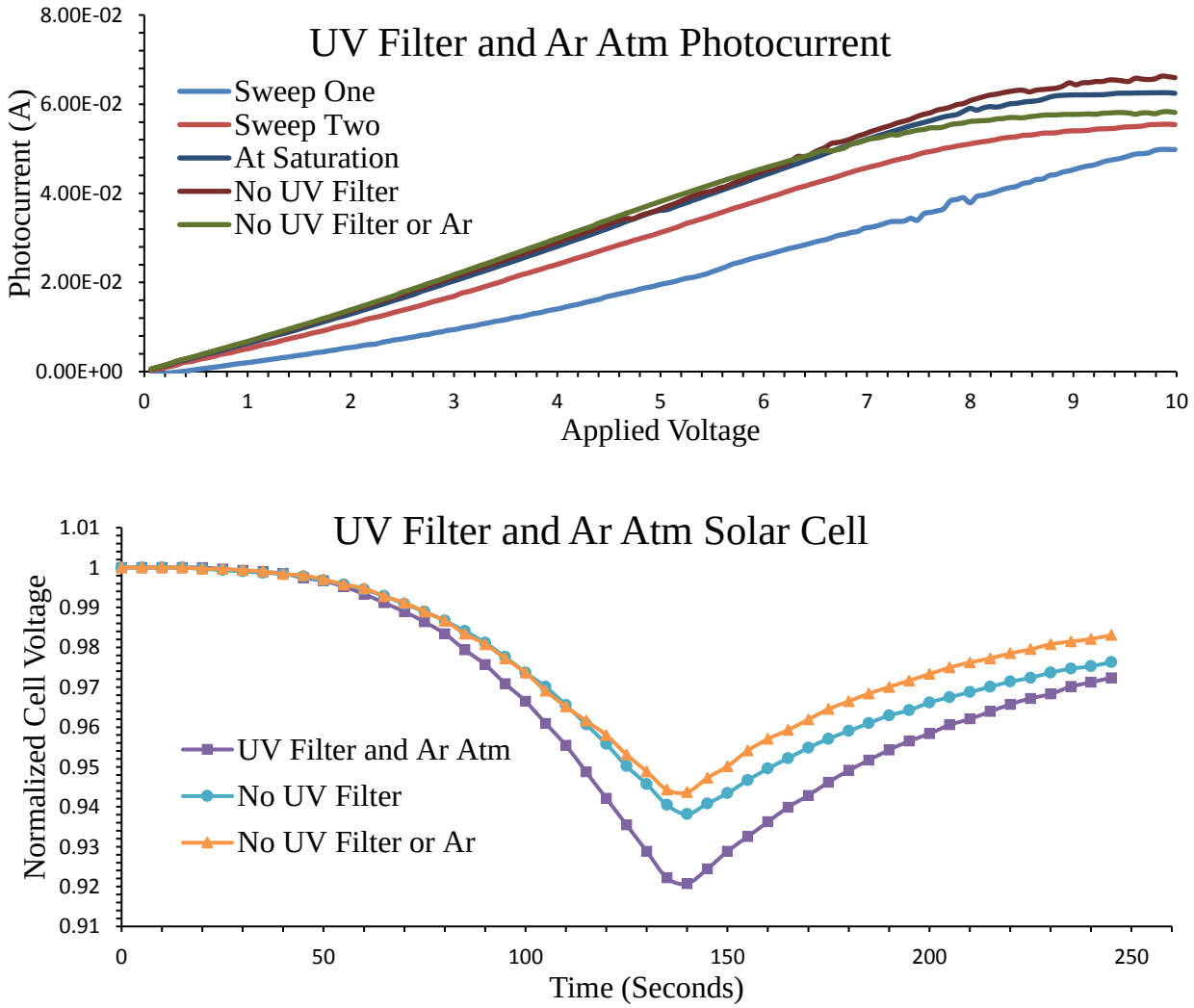

Figure 2.18. (Top) I-V curves for UV filter and Ar Atm combined trials. (Bottom) Solar cell voltages of UV filter and Ar Atm combined trials.

Finally, after the previously described trial, the argon was flushed from the sample holding box during recovery time. The following bias application resulted in a photocurrent which was lower than even the saturation value. This was likely due to the oxygen atmosphere oxidizing the zinc oxide, which made the nanostructures more resistive to current flow. It could be that this photocurrent value was very similar to the saturation value of a control experiment. The differences were similar to the differences in Figure 2.8, only in reverse order.

The solar cell voltage measurements also reinforced previous experiments. The trial labeled "No UV Filter or Argon" could be treated like a control run under normal conditions. Working backward from that, the trial labeled "No UV Filter" had only the photodetector submerged in an argon atmosphere, and looked very similar to Figure 2.16. There was little difference between the cell voltages during most of the device voltage application but, as before, the values diverged near 10 V, during lag time, and during recovery (from 150 to 270 seconds) of the cell voltage. "UV Filter and Ar Atm" showed the most light-blockage of any experiment presented thus far, and seemed to have resulted from a combination of the light interference observed in the previous ultraviolet and argon atmosphere trials combined. The data seems to suggest that whatever light blocking mechanism was taking place, it greatly favored a low oxygen atmosphere and photon wavelengths specific to the absorbance of the zinc oxide nanostructures.

2.3.7. Sweep Rate Cell Measurements

Solar cell measurements from variable sweep rate experiments are shown in Figure 2.19. At higher rates of voltage application, generally less light was blocked from the solar cell. This trend followed from 0.2 to 0.075 V/s, but the run at 0.065 V/s showed a higher cell voltage than the run at .075 V/s. It was possible that there existed some ideal photodetector voltage application rate (between 0.065 and 0.075 V/s) which would have resulted in a minimum cell

voltage measurement. Also important to note, for each trial the full 0-10 V bias was achieved, albeit at different time intervals.

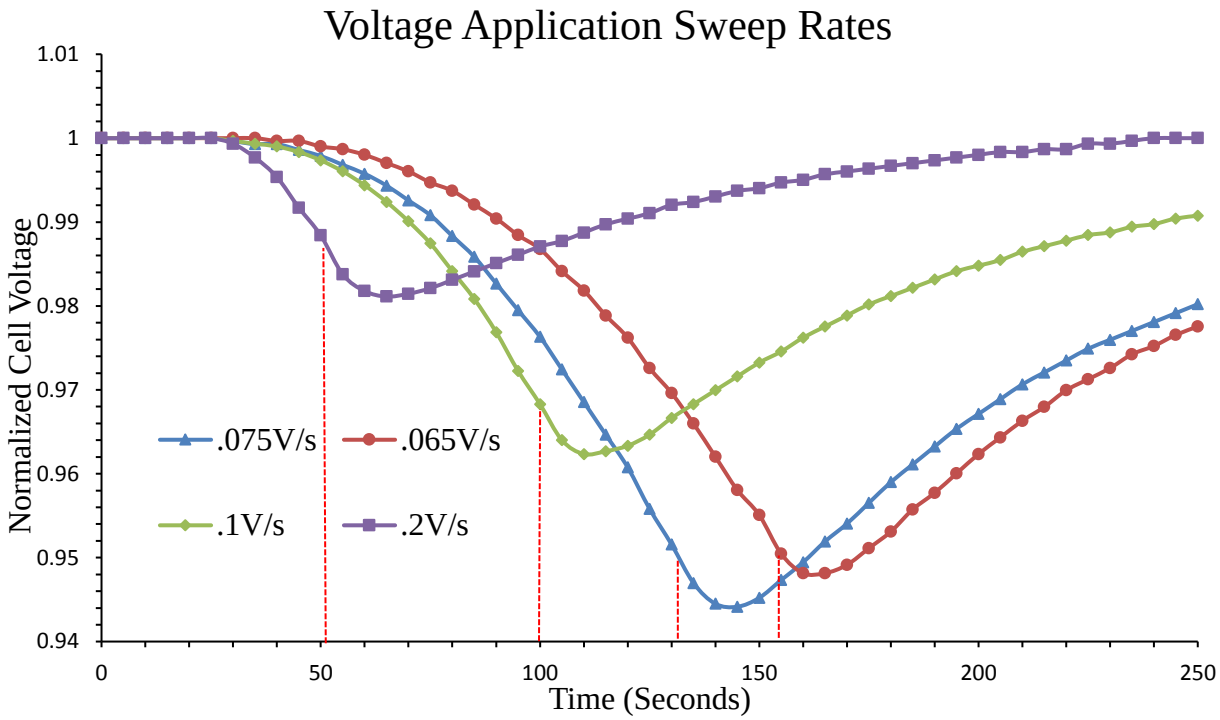

Figure 2.19. Solar cell voltages of different rates of voltage application.

Thus, the data from this figure indicates that it was not the specific electrical potential value, but instead the time frame over which the photodetector was exposed to the bias voltage which was directly responsible for interfering with the transmitted photons. If the device voltage value was the direct cause of photonic interference, each trial would have resulted in a very similar minimum cell voltage value, regardless of sweep rate. In regard to solar cell lag time, the values for sweep rates of 0.2, 0.1, 0.075, and 0.065 V/s were: 15, 10, 10, and 7 s, respectively. The voltage stop times are indicated in the figure by dashed red lines. This means that, in general, lag time varied inversely with the bias voltage sweep rate.

2.3.8. Variable Device Temperature Cell Measurements

It is well known that heated objects can scatter incident light. An everyday example of this phenomenon can be seen in the blurry region above hot asphalt. With this knowledge, it was hypothesized that perhaps heat scattering was the primary cause of the solar cell voltage drop observed during device voltage application. There was, after all, a large potential being applied to the very small surface area of the photodetector and a decent amount of current passing through the even smaller active area of the device. According to data from the device surface temperature measurements, the general trend was that the device was heating up during voltage application. If heat scattering was the primary cause of light interference through the photodetector, then most of the phenomena observed would be conisdered trivial and the research would have been superfluous.

Figure 2.20 shows the solar cell measurements from the temperature experiments. It is easily seen that there was a difference in cell voltage between the control and cooled trials. If heat scattering were the cause of light interference, then an increase in device temperature should correspond to a decrease in solar cell voltage. This is certainly seen by the overall shape of the cell voltage measurement graphs; as applied voltage increased toward 10 V, the cell voltage decreases. In comparing the "Control" with the "Cooled" trial, the device temperature measurements from Figure 2.11 did show a higher normalized temperature during "Cooled" and this corresponded to a lower cell voltage in Figure 2.20. However, the "Cooled_2" trial had a very similar maximum normalized temperature measurement to the "Control" trial, but also resulted in an identical cell voltage measurement to the "Cooled" trial below. Since the normalized solar cell voltage of the cooled trials decreased faster than the control trial it can be concluded that device heat scattering was not directly related to the light interference observed.

If device temperature was not the reason for photonic interference, the exact cause was

unknown. In the temperature experiment described above, the device was under constant argon flow, and the only variable was the use of liquid nitrogen to chill the flowing argon. As previously mentioned, due to inaccuracies in measuring the surface temperature of the device, it could not be determined if the device was sufficiently cooled by the chilled argon, so the decrease in cell voltage seen in Figure 2.20 could not be directly attributed to a change in device temperature. Thus, two possibilities remained: the device was being cooled by the chilled argon, but the temperature was not measured correctly; or, there was some other mechanism which was contributing to the decrease in cell voltage during the "Cooled" and "Cooled_2" trials. If the device was being cooled as intended, then the solar cell voltage decrease could have been a direct result of lower temperatures, but this would seem to contradict Figure 2.17 where an increase in the light source intensity would certainly have increased the device surface temperature. Thus, the totality of data collected seemed to point to another, non-temperature dependent mechanism of photonic interference.

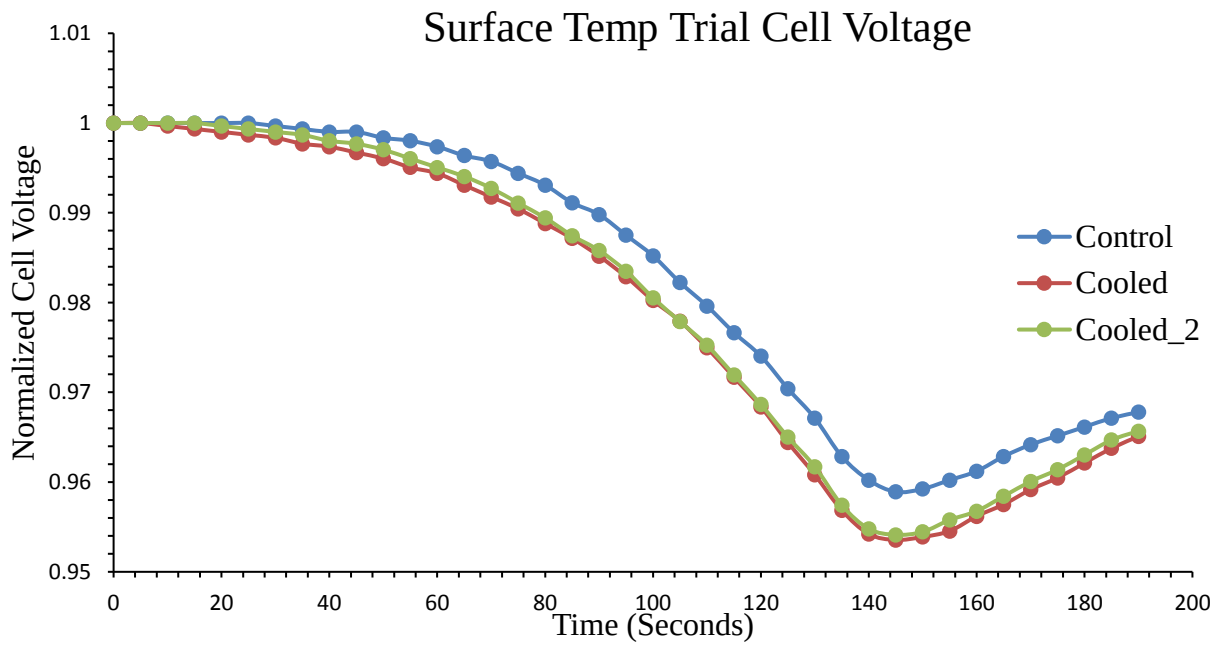

Figure 2.20. Solar cell voltages of control and cooled device trials.

2.4. Additional Experiments

2.4.1. Dynamic Solar Cell Trials

Another experiment which was performed involved an application of control bias conditions to the photodetector while the voltage of the solar cell was measured and the solar cell itself was kept at some distance from the device. In all previous trials, the solar cell was in direct contact with the back of the photodetector, however, it was necessary to determine if the same light blocking phenomenon could be observed for a small space between. Figure 2.21 shows the normalized solar cell voltage measurements of a control run, and two runs in which the solar cell was at a distance of 1-2 mm from the back of the device during voltage application. The figure shows that even at a distance of 1 mm, the change in solar cell voltage was far less and this trend continued at 2 mm. It could be extrapolated that at about 4-5 mm separation, the light blocking effect would be negligible. This data indicates that the light blocking phenomenon was a very near-field one, where over half the effect was unmeasurable within the first millimeter of distance from the back of the device. It should be noted that due to the design of the sample holder, there was very little light which reached the solar cell that had not also gone past the zinc oxide nanostructures and through the photodetector.

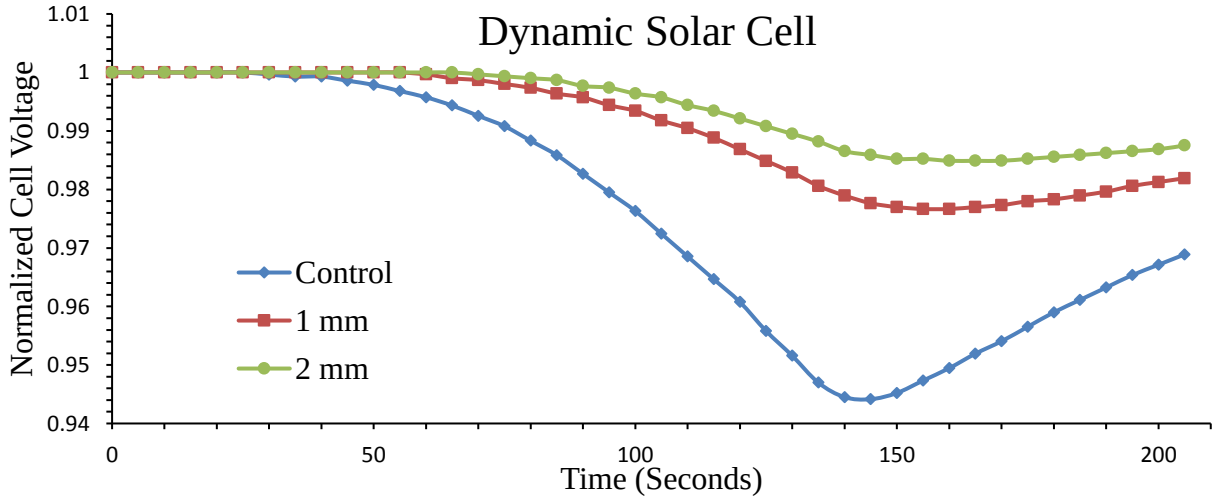

Figure 2.21. Solar cell voltages at various distances between device and solar cell.

2.4.2. Alternating Current (AC) Trials

Every previous voltage application had been done under a 0-10 V sweep which produced a direct current. In this experiment, the zinc oxide device was attached to an AC generator which applied 9 V of variable frequency. Both the photocurrent of the device and voltage of the solar cell were continuously measured with two different multimeters. The solar cell voltages of AC frequencies from 1-50 kHz are shown in Figure 2.22. It can be seen that frequencies of 16 kHz and 30 kHz corresponded to the most light-interference, while at the high and low end (1 and 50 kHz) the least amount of light-interference was observed. The photocurrent measurements were constant for each frequency setting and had values of 38.5, 42.6, 52.2, 0.4, and 5.93 mA for 1, 10, 16, 30, and 50 kHz, respectively. Frequencies above 50 kHz resulted in the current being too low to measure. Interesting to note was that under 16 kHz, the photocurrent was highest and cell voltage was lowest.

One possible explanation comes from what is known as the "skin effect", where, if the current running through a conductor varies sufficiently over time, it will be confined near the surface of that conductor. If the frequency of the alternating current is high enough, the electrons will be further confined to a very thin layer on the conductor surface. This effect is more pronounced in ferromagnetic materials, which includes zinc oxide [38, 39]. The skin effect is typically discussed as it pertains to materials which have larger-than-nano-sized dimensions, however, if it was present in the nanomaterials in this study, then it might explain why at higher frequencies the current approached zero. If the moving charges were being confined into a thin layer at the surface of the conducting material, and those materials were nano-sized, there might not have been enough volume for the charges to move, thus resulting a photonic blockage phenomenon.

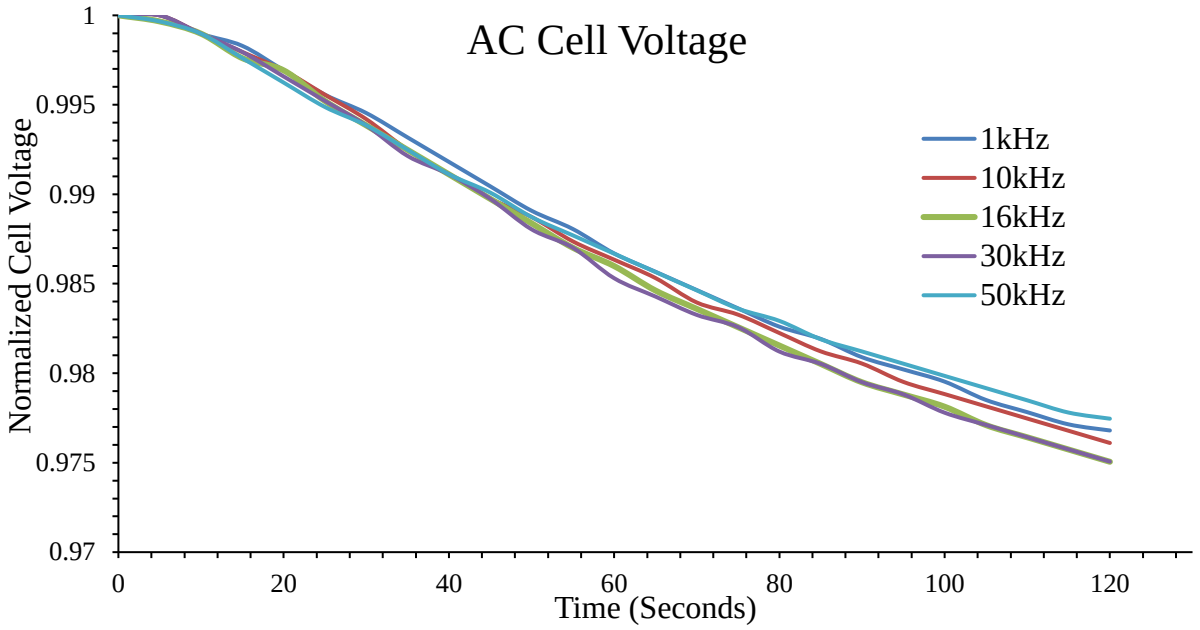

Figure 2.22. Solar cell voltages at difference sweep rates.

2.4.3. Alternate Device Confirmation

Another zinc oxide photodetector device was constructed for the purpose of confirming both the variable photocurrent and light interference phenomena. It was necessary to ensure that the primary device characteristics were not unique to its own construction and could be reproduced. Figure 2.23 shows the alternate device I-V characteristics were similar to the primary one.

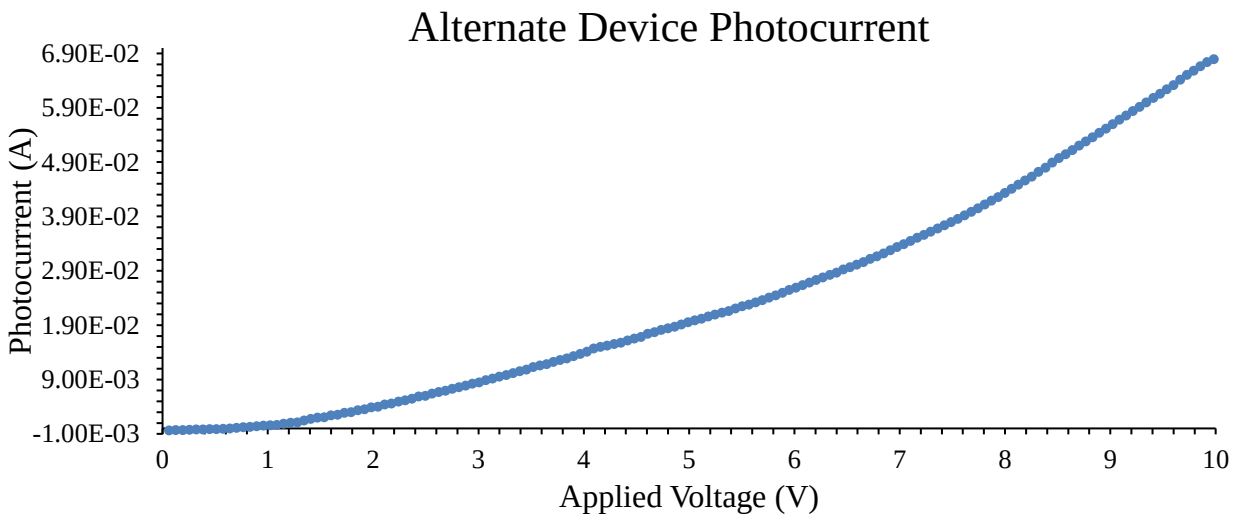

Figure 2.23. I-V curve of alternate, confirming device.

Similar photocurrent variability, saturation, and light-interference were also observed in the alternate device. Differences in the specific shape and maximum value of the photocurrent were due to slight inconsistencies in the electrode orientation and local densities of the zinc oxide nanostructure growth.

2.4.4. Additional Nanostructured Devices

In observing and measuring the phenomena associated with the primary branched nanostructured devices, in was necessary to determine if those characteristics were unique to the specific set of nanostructures which were used. Thus, as an additional facet to the research, two other unique sets of zinc oxide nanostructures were hydrothermally grown onto two different photodetectors. The first new type of nanostructures was an array of dense, single nanorods; the second type were called "nano-flowers". SEM images of these alternate morphologies are shown in Figures 2.24 and 2.25.

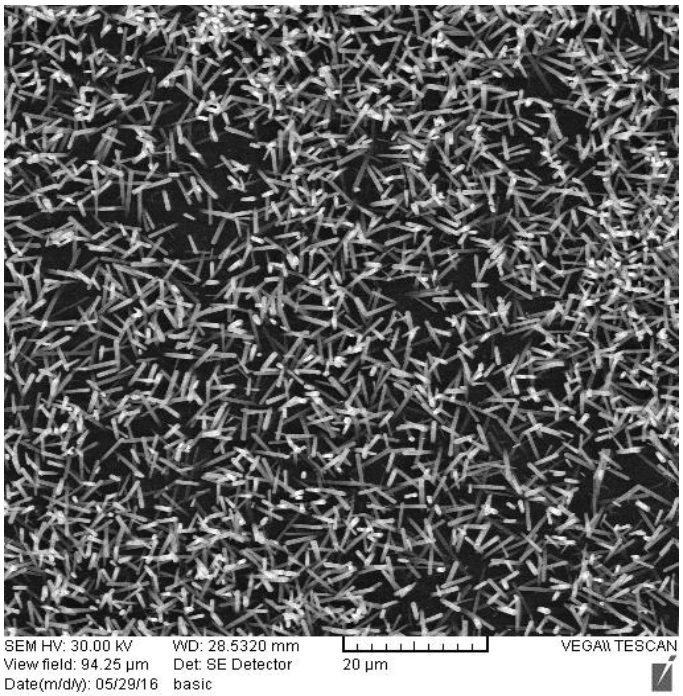

Figure 2.24. SEM image of hydrothermally grown zinc oxide nanorod field.

The nanorod array was grown similar to the initial, single rod structure used for the primary device, but the increased density of the rods was due to an initial seed layer, grown using a slightly modified technique from Wang *et al* [40]. The nanoflowers were grown by a single hydrothermal step involving equimolar zinc nitrate and HMT and 70 µL of DAP; the same as the last step for the primary nanostructures.

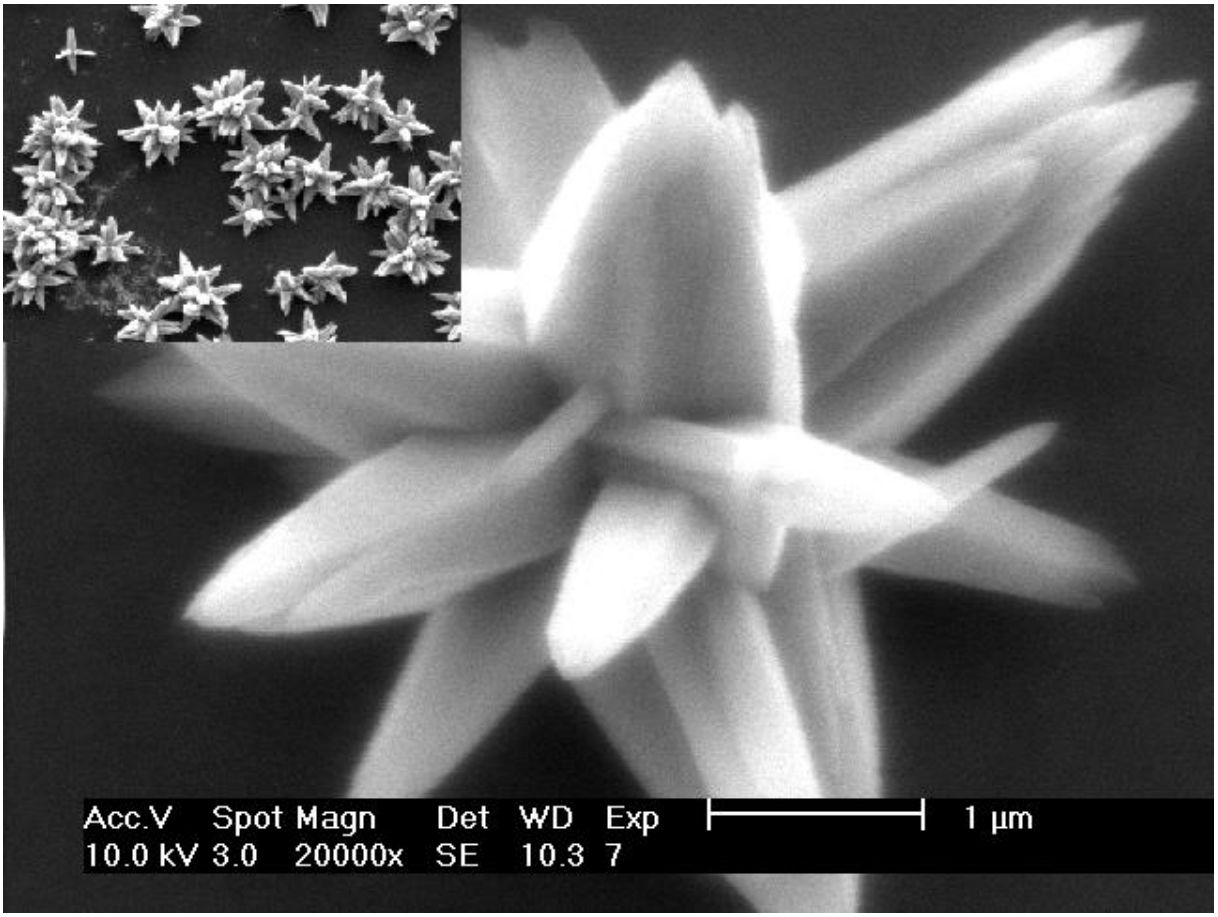

Figure 2.25. Zoomed SEM image of hydrothermally grown zinc oxide nanoflower (main) and nanoflower field (window).

These different nanostructures were grown with the intention of determining if the variable photocurrent and light-interference mechanisms were dependent on morphology of the micro/nano-scaled zinc oxide and what, if any, phenomena changed along with changing zinc

oxide shape. The nanorod array and nano-flowered photodetectors were subjected to the same experiments as were the primary nanostructures to confirm or deny similar behavior. However, for the construction of these devices, the nanostructures were grown on recycled photodetector bases as opposed to having been constructed and grown from a blank quartz slide. This was necessary due to lab equipment malfunctions. Despite the setback, the devices were recycled via light acid bath to clean and remove the previous zinc oxide from the surface. This was followed by washing in deionized water, drying, and regrowth under normal, ideal conditions. The growth of the two sets of nanostructures were, nonetheless, confirmed by both optical microscope and SEM. The photocurrent saturation processes and solar cell measurements for the nanorod array and nanoflowers are shown in Figures 2.26 and 2.27, respectively.

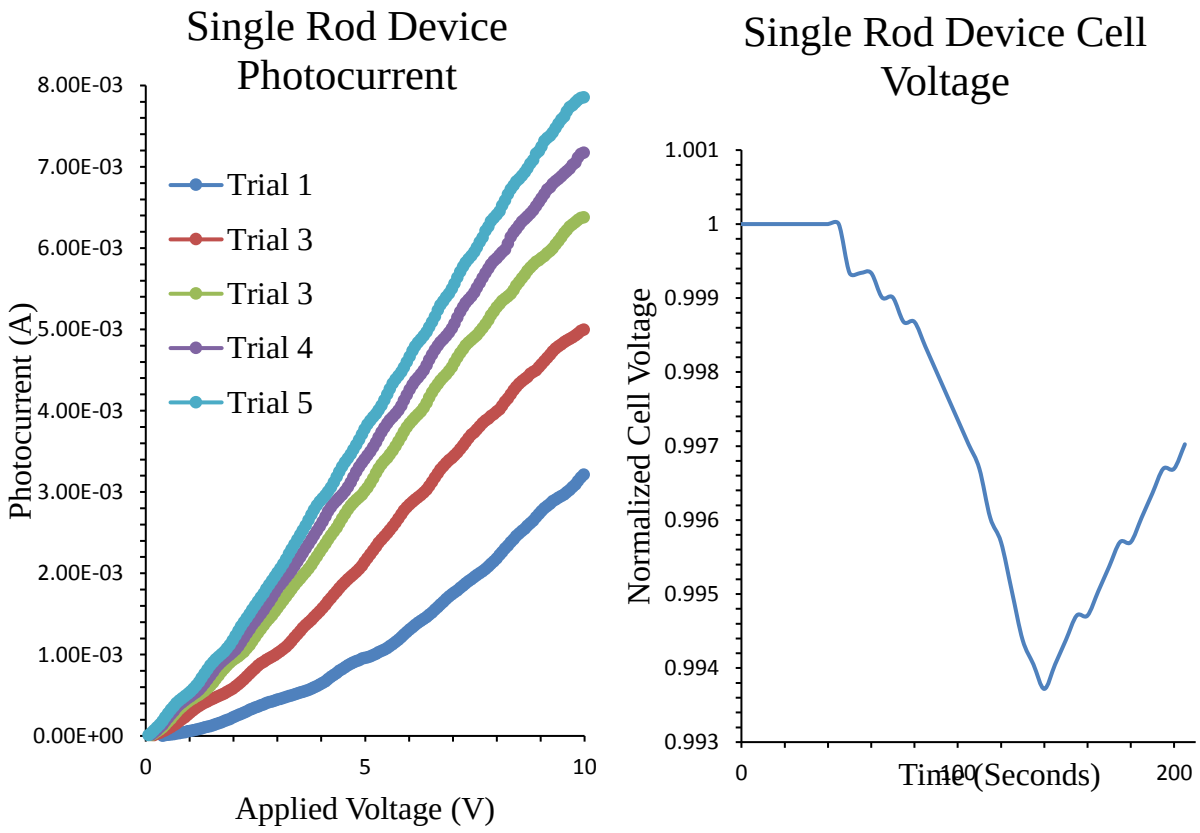

Figure 2.26. (Left) Saturation process of the single rod array device. (Right) Normalized solar cell voltage.

These graphs show that the photocurrent measurements of the two additional devices remained at a far lower level than those seen in the primary device; however, the saturation process was still evident. The photocurrent trends (associated with increased intensity, inert atmosphere, and ultraviolet filtered experiments) observed in the primary device were also seen in the two additional devices, but to a somewhat lesser degree. Similar statements can be made about the devices' corresponding solar cell voltages: the phenomena were present, but were observed to a lesser extent. There did appear to be a slight difference between the single rod and nanoflower devices, however, as shown in Figure 2.27. The device which was grown with the nanoflowers showed both a higher maximum photocurrent and a lower normalized solar cell voltage during external voltage application as compared to the single rod device. Similar trends to the primary photodetector were also seen in the device solar cell voltages confirming the presence of the light-interfering mechanism, albeit a lesser one.

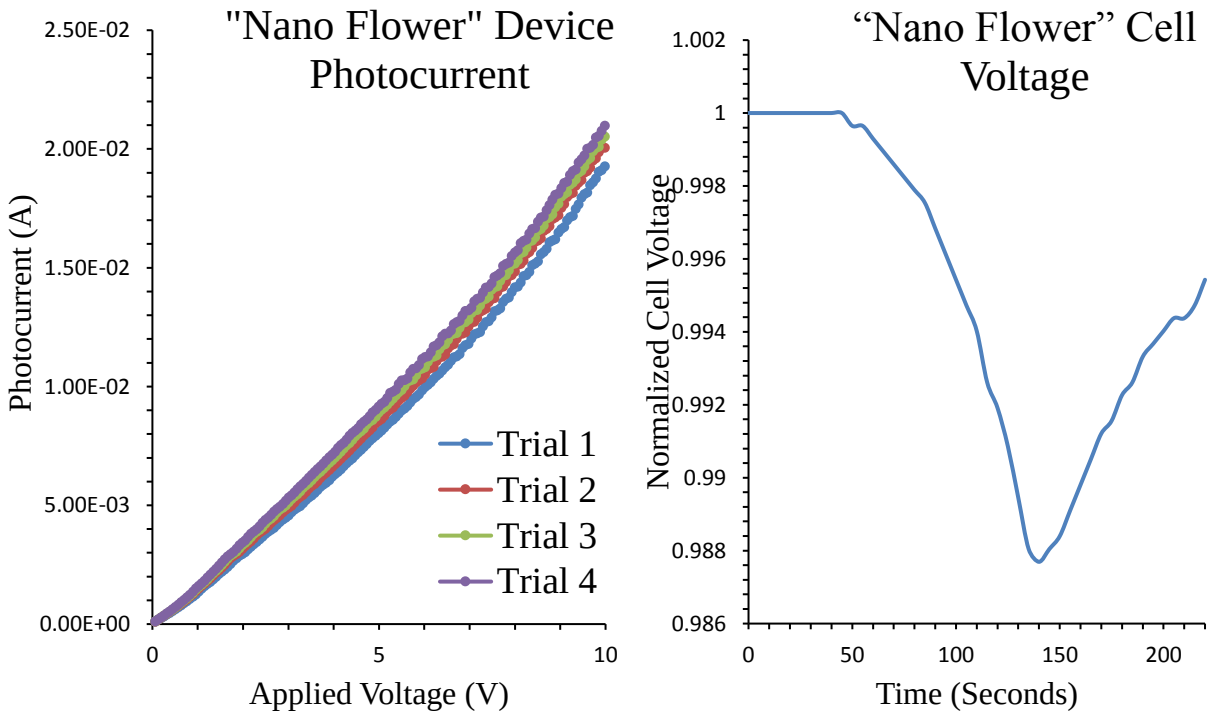

Figure 2.27. (Left) Saturation process of the nanoflower device. (Right) Normalized solar cell voltage.

Results and Discussion

3.1. Zinc Oxide Oxygen Surface states

The experiments performed represent a systematic analysis of a specific family of zinc oxide nanostructures. The key results from experiments, which regarded device photocurrent as a function of applied potential, were that the photocurrent was variable and could be altered by factors such as increased light intensity and a change of the ambient atmosphere. It was likely that most of the variations in photocurrent were due to surface oxygen states which had either left or become trapped within the surface of the zinc oxide. This was most notably the case in the variable atmosphere trials where the change in ambient oxygen concentration was likely directly linked to oxidation of the nanostructures which resulted in changes in photocurrent. This oxidation of the nanostructures was further changed by variables such as consecutive voltage applications, time between applications, and temperature. Laio *et al* reported on a similar phenomenon and attributed it to the absorbed surface oxygen states which could trap free electrons resulting in variable photocurrent [41].

Furthermore, it could be hypothesized that during application of a bias voltage, a photocurrent was produced and the charges were confined to move through the small volume of the nano-branched structures. This large relative current which moved through the nano-sized zinc oxide could have transferred some of its energy to the oxygen atoms on the nanostructure surfaces. The newly energized oxygen atoms could then easily diffuse from the zinc surface. As more oxygen left the surface, the zinc oxide became less resistive and allowed more photocurrent to flow.

In the case of the variable atmosphere experiments, the change in photocurrent could be described by direct diffusion of oxygen rather than an energized release. During a control

voltage application, it could be inferred that the oxygen in the atmosphere and that on the surface of the zinc oxide was near an equilibrium value. Any oxygen released from the surface could have been due to the excitation by the photocurrent, as described above. However, if the photodetector had been biased in the presence of an oxygen-deficient atmosphere such as argon or nitrogen, there would have been a large gradient between the oxygen in the nanostructures and that in the atmosphere. Thus, the more highly concentrated oxygen on the zinc oxide surface would have been more likely to diffuse off the surface of the nanostructures and out into the less concentrated atmosphere. As before, with fewer oxygen atoms, the zinc oxide became less resistive and resulted in a higher photocurrent, as shown in Figure 2.9. The opposite effect was seen in an oxygen-rich atmosphere. There was a larger number of oxygen molecules in the atmosphere than on the zinc oxide nanostructures, which enabled the atmospheric oxygen to diffuse onto the surface of the nanostructures. The increased oxidation led to more resistivity and less photocurrent.

These hypotheses do address the photocurrent variations in their respective experiments, but they may not fully explain the effects which were present during every individual experiment; for example, the saturation phenomenon and saturation trend effects which were subtly present in all of the experiments described. While it could be surmised that an overall decrease in the oxygen states within the zinc oxide nanostructures was responsible for the saturation process, the question remained why there had to be a specific amount of time between voltage applications in order to yield the maximum possible photocurrent, e.g., saturation/recovery time. Recall from Figure 2.6 that the time between voltage applications was the time allotted for the voltage of the solar cell to return to the initial value. It was found that this time was needed not only to allow the cell voltage to return to a steady state value, but also allowed the most gain in maximum

photocurrent between applications if not previously at saturation, or kept the photocurrent at the saturated value. If it is to be hypothesized that the energy from the photocurrent was aiding in oxygen diffusion, then more current should mean more diffusion and the least amount of oxygen in the zinc oxide after a voltage application. Thus, in this minimal oxygen regime it would stand to reason that if a consecutive voltage application was immediately applied, it would have only furthered the diffusion of oxygen off the zinc oxide, and resulted in another increase in maximum photocurrent. Experimentally, however, if the device was at saturation, this was not the case.

This leads to two possible conclusions. One conclusion is the diffusion of oxygen was not present at all during these experiments, and some other method entirely was responsible for the variations in photocurrent. This seems unlikely as diffusion of oxygen agrees with the measured data. The second conclusion is that diffusion of oxygen was present and accounted for most variations in current, but there must have been an important action taking place directly after voltage application. Looking at a point in time just before 10 V was reached and the voltage application and photocurrent stopped, the conditions were as such: a strong electric potential was present across the nanostructures, a maximum current flowed, and oxygen states in the zinc oxide were at a temporary minimum. At 10 V, everything stopped. Presumably at that point, since the zinc oxide was deficient in oxygen, there existed a gradient between the nanostructures and the atmosphere. If a gradient was present, then diffusion should take place in the opposite direction, back onto the nanostructures. Thus, if the voltage application was immediately begun, perhaps there would have been less diffusion from the zinc oxide since the atmospheric oxygen was still in the process of diffusing back onto it, which resulted in a lesser change in the number of oxygen atoms in the zinc oxide and a lower photocurrent.

A variation on this hypothesis would be that once 10 V was reached, the current stopped, and there was a gradient between the nanostructures and atmosphere. Oxygen then rapidly diffused back onto zinc oxide, rather than slowly. Because of this rapid diffusion, the oxygen concentration in the zinc oxide could have reached a higher than equilibrium amount. This condition could have then led to a slow oxygen diffusion back off the ZnO and into the atmosphere as equilibrium was reached. With enough recovery time for the oxygen to have reached the optimal control amount, the next voltage application would see a sufficient photocurrent-induced oxygen diffusion and a higher or equal maximum current value, depending on if the device was at saturation or not. If, instead, no recovery time had been allowed, there would not have been enough time for the oxygen concentration to reach the equilibrium value, which resulted in higher than optimal oxygen levels and less photocurrent. This hypothesis presents the idea that there was an equilibrium concentration of oxygen in the nanostructures; that level decreased during saturation and remained at a steady minimum once saturation had been reached.

3.2. Variable Transmission Through Zinc Oxide

Perhaps the most intriguing and confusing phenomenon observed in this series of experiments was the variability of transmission through the photodetector device under differing experimental conditions. Looking at Figure 2.13, it can be seen that the initial indication of light-interference occurred around 3-4 V as evident by the solar cell voltage drop. At a higher bias the cell voltage continued to drop at an increased rate. In order to provide a better understanding of the experimental environment, the state of events can be described as follows: an electric field formed between the gold electrode fingers, charges were generated from the zinc oxide nanostructures by the ultraviolet range of wavelengths from the light source (some also

from heat), and the generated electrons moved due to the electric field which resulted in a photocurrent. As the applied electric potential increased, the charges moved faster, which generated an even higher current. Incoming photons from the solar simulated light source reached the photodetector, moved in proximity to the zinc oxide nanostructures, and those which weren't directly absorbed or reflected, transmitted through the quartz to be absorbed by the solar cell.

Data indicated that during the time the incident photons were in proximity to the nanostructures, while the bias was in place and charges were moving between the gold electrodes and through the zinc oxide, some of the photons failed to make it past the zinc oxide, through the quartz substrate, and to the cell. Figure 2.14 had already disproven the notion that the amount of photocurrent was directly related to the interference of photons, thus, there must have been some other mechanism which caused the effect. Upon examination of the data from Figures 2.15 and 2.16, it can be seen that with the addition of the experimental variables there was a noticeable change in the approximate percentage of light which transmitted to the solar cell during voltage application. In the case of the ultraviolet filtered trials, the cell voltage differences between the control and filtered trials were evident throughout most of the voltage application. Near 5 V, the trials with the ultraviolet filter began to show a greater decrease in the solar cell voltage. The faster rate of decrease continued until the voltage application stopped, after which time the filtered trials reached a lower minimum than the control trial.

This indicated that the ultraviolet range of light was more susceptible to the observed light interfering mechanism. Even though the same wavelength range of light was present in the control trial (in addition to the rest of the solar spectrum) and reacted to the interfering mechanism, perhaps the other wavelengths of light from the light source were not as affected,

which kept the cell voltage at a higher value throughout the sweep. If the remaining, non-filtered ultraviolet wavelengths were more affected by the light interfering mechanism compared to the other wavelengths, then it further connects this phenomenon to the specific family of zinc oxide nanostructures used for this research.

Looking at the variable atmosphere experiment results in Figure 2.16, it can be seen that the difference between the control and argon ambient trials was only evident during the "lag time" period. Prior to that, the solar cell voltage appeared consistent between the two trials. This data is important as it suggests that the photonic transitivity through the device in an inert atmosphere was not differently affected by the light interfering mechanism compared to in ambient atmosphere; however, whatever the cause of photon interference, it was more sustained after the bias application stopped in the inert atmosphere as seen by the lower minimum cell voltage. The primary result of the device operating in an inert atmosphere was less oxidation of the nanostructures, and the cell voltage graph showed that there was a significant difference between the lag time behaviors of the control and inert atmosphere trials. Most noticeable was the lag time lasted a couple of seconds longer and resulted in an overall lower approximate percentage of transmitted photons.

Thus, the data could suggest the possibility that variable oxidation of the zinc oxide nanostructures might have had some effect on the light interfering mechanism, and the two could be directly related. This conjecture could only be valid during the lag time period since that was where the differences between the two trials occurred. Another idea is that the argon absorbed more light during device voltage application; however, if this were the case, the graph would have shown a greater decrease in cell voltage over the entire bias application. To generalize these results, a change in the wavelength or intensity of the incident light altered the photonic

susceptibility to the light blocking mechanism; whereas a change in atmosphere or temperature altered the light blocking mechanism directly.

Photons must have been either scattered/blocked or were being absorbed/trapped by the nanostructures. If scattered/blocked what obstacle impeded the photons? If absorbed, how were the nanostructures further absorbing the photons past the normal, expected, UV absorption? The results from the experiments led to these questions, but no answers were determined.

3.3. Additional Experimental Results

The data from the ultraviolet/argon combined trials helped reinforce previous suggestions about surface oxidation and wavelength dependence. Results from the dynamic cell experiment suggested the light blocking mechanism was very short-ranged. The dependence of light-interference on the duration of a certain voltage was applied could be seen from the variable rates of bias sweeps. With the addition of alternating current, light-interference was variably dependent on frequency, which was related to the speed of the current. If there was a direct relationship between these two factors, then it again suggested that it was not the amount of current which determined how much light was blocked, but was instead how fast the charges were moving and how long they were exposed together.

Finally, the data from the two additional nanostructured photodetectors gave some small, but informative results. Both devices showed that the photocurrent variability as well as light-interfering mechanism were not completely unique to the branched nanostructures in the primary device. With that said, the phenomena observed in the additional devices was extremely minute. This drastic difference could have been due to two possibilities. The first is that the two additional nanostructures had sufficiently different morphologies from the primary nanostructures that the phenomena occurred under less than ideal conditions, but were still

measurable. The primary difference between all three sets of nanostructures was the surface area to volume ratios. Most likely, the primary nanostructures had the largest ratio, with the single rod arrays having the smallest. This is reflected in Figure 2.26 which showed the lowest current and highest remaining normalized cell voltage. Thus, the conclusion could be drawn that a high surface area was ideal to observe the maximum effect.

Conversely, the second possibility is that the differences measured between the two additional devices and the primary device were due to slightly different photodetector construction methods. As mentioned previously, these devices were constructed from recycled samples. The confirmed optimal growth of the new nanostructures ensured that the cause of the lesser photocurrents and light-interference was more likely due to electrode degradation of the recycled devices rather than issues with the nanostructures.

Still, considering Figures 2.26 and 2.27, and keeping in mind that a difference in surface area can lead to differences in the observed phenomena, it may be hypothesized that the ideal conditions for maximum observation and measurement would be a high surface area with small feature size. Both the primary branched nanostructures and nanoflowers have nano-scaled features, and this seemed to have been key in facilitating the most light-interference. While these results do not directly provide additional information regarding what caused the photonic interference, they have shown what can further the persistence of the phenomenon: surface area and feature size.

4. Conclusions and a Forward Look

4.1. Research Conclusions

This research represents a series of methodical and systematic experimental trials on a simple, novel ultraviolet photodetector designed to give understanding behind the optical and electrical phenomena observed in a small set of zinc oxide nanostructures. The data suggested that some of the oxygen atoms on the surface of the zinc oxide structures could be removed, with some degree of predictability, via application of a linear voltage rate across the electrodes of the photodetector, as well as through other experimental conditions. This ability to tune the oxidation of the semiconducting material in order to yield an, also somewhat predictable, photocurrent, could potentially pave the way for application in electronics such as more sophisticated photodetector or sensors. A better understanding of what mechanism(s) influence oxidation can lead to more efficient utilization of those mechanism in said devices.

Also under experimental examination, was the phenomenon by which the incident light's variable transmission past the zinc oxide nanostructures and through the photodetector substrate was a function of the photonic wavelength, photonic density, ambient atmosphere, ambient and device temperature, voltage application rate, time between applications, frequency of alternating current, and electric field strength. The exact source of the light interference mechanism and has yet to be understood, but some ideas have been proposed. Data from the systematic trials supported the variable oxidation of the zinc oxide nanostructures as having a possible connection to the light interference, but might not have been the only affecting factor. Further data has led to the hypothesis that the speed of the moving charges through the limited dimensions of the nanostructures was at least partially responsible for photonic interference.

4.2. Possible improvements

In regard to the previously described research performed, data can only be as good as the equipment used to gather it. Most experimentation can be improved upon to get more accurate results, and the research detailed in this paper was no exception. Sometimes, however, one must make use with the resources currently at hand, while keeping in mind ideal experimental conditions and equipment. Some techniques and equipment improvements for the mentioned research are as follows. Primarily, it would be beneficial to have constructed the photodetector using more sophisticated methods to better control the consistency of the device dimensions. Vapor deposition or optical lithography methods for forming the gold interdigitated electrode pattern would ensure more even distribution, allow for smaller electrode finger dimensions, and ensure a more stable layer. The ideal design for this photodetector which would give the clearest results would involve a wider, opaque central opening, where the zinc oxide nanostructures would be grown between longer, narrower, and more dense electrode fingers. The thin, dense fingers wouldn't block much incoming light, but would provide a maximum surface area to connect to the nanostructures. This should further increase the phenomena observed in previous experiments by packing more nanostructures for the electrons to interact with between the electrode fingers, but still leave room for transmission.

Also, the practice of using thin copper masks to form the gold electrode design was often an arduous and unproductive task. The incredibly thin masks were difficult to handle and place, making the assembly process unnecessarily lengthy. In addition, due to their thinness, they were very fragile; small bends or chinks in the masks led to an nonuniform surface morphology. Any irregularity could result in a misaligned electrode finger, which would then create a short between the opposing electrodes. Combined, these factors occasionally made the already lengthy device construction unsuccessful, or at the least, produced a somewhat inefficient

product. As a general rule of device fabrication, more control over the design and construction process translates to more control over the characteristics of the device, more reproducible results, and overall better operating parameters.

More reliable measuring equipment would also be useful. Automating the solar cell voltage and surface temperature measurements would remove human error associated with manual readings and handling and add more precision and reliability to the data. Also, a better sealed housing unit for ambient trials would ensure an "oxygen deficient" atmosphere was more controllable.

4.3. Looking Forward in this Research

It would be of interest to continue the research detailed in this paper so that a more complete understanding could be achieved. The research described here only scratched the surface of these fairly new nanostructures and their unique optical and electrical properties. Many more studies must be conducted before the phenomena can be fully comprehended and put to technological and industrial use. These would include the growth of other zinc oxide nanostructures available for synthesis, such as nano-wires, nails, tetrapods, rings, springs, etc. in in addition to the nanostructures studied here. It is necessary to determine the dependence the observed phenomena have on the nanostructures morphology. Perhaps some other zinc oxide nanostructure better exhibits the observed effects described here, and would make a better candidate for use in the optoelectronic field; or, perhaps the synthesized nano-branched structures used here are the ideal structures, in which case, further study would be needed to determine the optimal growth parameters and dispersion patterns.

While the solar cell used in the described research was sufficient for measuring approximate percentages of transmitted light, it had limitations and was not highly accurate. A more accurate

light measuring device would provide much more precise information and, if a spectrometer were to be used in addition, the transmitted light intensity as well as specific wavelengths could be measured as a function of bias voltage.

Zinc oxide has been doped with many different metallic elements such as aluminum, iron, copper, etc., with the outcome being altered optical and electrical properties [42, 43]. Thus, it would be of interest to explore the effects of doping on the variable photocurrent and light interference phenomena. Furthermore, it could be incredibly informative to perform some of the previously described experiments under a vacuum. Doing so could shed more light on the possible link between variable surface oxidation diffusion and the light interference mechanism.

Zinc oxide, its nanostructures, and their ultraviolet absorption/light blocking properties have the potential to be utilized in new materials and devices. An example of such new, possible technology includes car windshields imbedded with zinc oxide nanostructures which, when subjected to an electrical bias and sufficient ultraviolet light, could block some of the incident radiation thereby shielding the driver and passenger from the harmful or blinding effects of sun light. This same technique could be used in sunglasses or in the large windows of skyscrapers. The outcome of these applications could be added human protection from ultraviolet radiation from the sun, or even more efficient and convenient solar energy harvesting.

References

[1] S. M. Sze, "Semiconductor Devices Physics and Technology", 2nd ed., *John Wiley and Sons Inc*., 2002, pages 28-37, 60-63, and 225-236.

[2] K. Seeger, "Semiconductor Physics An Introduction", 7th ed., *Springer*, 1999, pages 1-16 and 34-35.

[3] B. Sapoval and C. Hermann, "Physics of Semiconductors", 1st ed., *Springer*, 1995, pages 27-30, 41-46, and 65-77.

[4] S. Talam, S. R. Karumuri, and N. Gunnam, "Synthesis, Characterization, and Spectroscopic Properties of ZnO Nanoparticles", *ISRN Nanotechnology*, Vol. 2012, Article ID 372505, pages 1-6, 2012.

[5] G. Chai, O. Lupan, L. Chow, and H. Heinrich, "Crossed zinc oxide nanorods for ultraviolet radiation detection", *Sensors and Actuators A: Physics*, Vol. 150, pages 184-187, 2009.

[6] X. W. Sun, S. F. Yu, C. X. Xu, C. Tuen, B. J. Chen, and S. Li, "Room-Temperature Ultraviolet Lasing from Zinc Oxide Microtubes", *Journal of Applied Physics*, Vol. 42 pages 1229-1231, 2003.

[7] A. Janotti and C. G. Van de Wall, "Fundamentals of zinc oxide as a semiconductor", *Reports on Progress in Physics*, Volume 72, Number 12, 2009.

[8] Z. Fan and J. G. Lu, "Zinc Oxide Nanostructures: Synthesis and Properties", *Journal of Nanoscience and Nanotechnology*, Vol. 5, No. 10, pages 1-13, 2005.

[9] Z. L. Wang and J. Song, "Piezoelectric Nanogenerators Based on Zinc Oxide Nanowire Arrays", *Science*, Vol. 312, No. 5771, pages 242-246, 2006.

[10] J. L. Deschanvres, P. Rey, G. Delabouglise, M. Labeau, J. C. Joubert, and J. C. Peuzin, "Characterization of Piezoelectric Properties of Zinc-Oxide Thin-Films Deposited on Silicon for Sensors Application", *Sensors and Actuators A-Physical*, Vol. 33, No. 1-2, pages 43-45, 1992.

[11] C. C. Hsiao and S. Y. Yu, "Rapid deposition process for zinc oxide film applications in pyroelectric devices", *Smart Materials and Structures*, Vol. 21, pages 1-7, 2012.

[12] A. Arnau, "Piezoelectric Transducers and Applications", 2nd ed., *Springer*, 2008, pages: 2-4.

[13] J. G. Webster, "The Measurement, Instrumentation, and Sensors Handbook", *CRC Press LLC*, 1999, section: 32.7.

[14] P. X. Gao and Z. L. Wang, "Nanoarchitectures of semiconducting and piezoelectric zinc oxide", *Journal of Applied Physics*, Vol. 97, 044304, pages 1-7, 2005.

[15] J. Y. Li, X. L. Chen, H. Li, M. He, and Z. Y. Qiao, "Fabrication of zinc oxide nanorods", *Journal of Crystal Growth*, Vol. 233, No. 1-2, pages 5-7, 2001.

[16] Y. Dia, Y. Zhang, Q. K. Li, and C. W. Nan, "Synthesis and optical properties of tetrapod-like zinc oxide nanorods", *Chemical Physics Letters*, Vol. 358, No. 1-2, pages 83-86, 2002.

[17] P. Ravirajan, A. M. Peiro, M. K. Nazeeruddin, M. Graetzel, D. D. C. Bradley, J. R. Durrant, and J. Nelson, "Hybrid Polymer/Zinc Oxide Photovoltaic Devices with Vertically Oriented ZnO Nanorods and an Amphiphilic Molecular Interface Layer", *Journal of Physical Chemistry B*, Vol. 110, No. 15, pages 7635-7639, 2006.

[18] Z. L. Wang, "Zinc oxide nanostructures: growth, properties and applications", *Journal of Physics: Condensed Matter*, Vol. 16, pages R829-858, 2004.

[19] S. H. Ko, D. Lee, H. W. Kang, K. H. Nam, J. Y. Yeo, S. J. Hong, C. P. Grigoropoulos, and H. J. Sung, "Nanoforest of Hydrothermally Grown Hierarchical ZnO Nanowires for a High Efficiency Dye-Sensitized Solar Cell", Nano Letters, Vol. 11, pages 666-671, 2011.

[20] W. J. E. Beek, M. M. Wienk, and R. A. J. Jassen, "Efficient Hybrid Solar Cells from Zinc Oxide Nanoparticles and a Conjugated polymer", Advanced Materials, Vol. 16, No. 12, pages 1009-1012, 2004.

[21] S. K. Hau, H-L. Yip, N. S. Baek, J. Zou, K. O'Malley, and A. K.-Y. Jen, "Air-stable inverted flexible polymer solar cells using zinc oxide nanoparticles as an electron selective layer", *Applied Physics Letters*, Vol. 92, No. 253301, pages 1-3, 2008.

[22] E. Hosono, S. Fujihara, I. Honma, and H. Zhou, "The Fabrication of an Upright-Standing Zinc Oxide Nanosheet for Use in Dye-Sensitized Solar Cells", *Advanced Materials*, Vol. 17, pages 2091-2094, 2005.

[23] T. Jin, D. Sun, J. Y. Su, H. Zhang, and H.-J. Sue, "Antimicrobial Efficacy of Zinc Oxide Quantum Dots against Listeria monocytogenes, Salmonella Enteritidis, and Escherichia coliO157:H7", *Journal of Food Science*, Vol. 74, issue 1, pages M46-M52, 2009.

[24] Y. Liu, K. Ai, Q. Yuan, and L. Lu, "Fluorescence-Enhanced Gadolinium-Doped Zinc Oxide Quantum Dots for Magnetic Resonance and Fluorescence Imaging", *Biomaterials*, Vol. 32, pages 1185-1192, 2011.

[25] Q. Huang, D. Zend, H. Li, and C. Xie, "Room Temperature Formaldehyde Sensors with Enhanced Performance, Fast Response and Recovery Based on Zinc Oxide Quantum Dots/Graphene Nanocomposites", *Nanoscale*, Vol. 2, pages 5651-5658, 2012.

[26] S. Roy and S. Basu, "Improved Zinc Oxide Film for Gas Sensor Applications", *Bulletin of Material Science*, Vol. 25, No. 6, pages 513-515, 2002.

[27] B. B. Rao, “Zinc Oxide Ceramic Semi-Conductor Gas Sensor for Ethanol Vapour”, *Materials Chemistry and Physics*, Vol. 64, pages 62-65, 2000.

[27] C. Gao, X. Li, Y. Wang, L. Chen, X. Pan, Z. Zhang, and E. Xie, “Titanium Dioxide Coated Zinc Oxide Nanostrawberry Aggregates for Dye-Sensitized Solar Cell and Self-Powered UV-Photodetector”, *Journal of Power Sources*, Vol. 239, pages 458-465, 2013.

[28] L. Qin, C. Shing, and S. Sawyer, “Metal–Semiconductor–Metal Ultraviolet Photodetectors Based on Zinc-Oxide Colloidal Nanoparticles”, *IEEE Electron Device Letters*, Vol. 32, No. 1, pages 51-53, 2011.

[29] E. Lee, D.-I. Moon, J.-H. Yang, K. Su. Lim, and Y.-K. Choi, “Transparent Zinc Oxide Gate Metal–Oxide–Semiconductor Field-Effect Transistor for High-Responsivity Photodetector”, *IEEE Electron Device Letters*, Vol. 30, No. 5, pages 493-495.

[30] B. E. A. Saleh and M. C. Teich, “Fundamentals of Photonics”, *John wiley & Sons, Inc*., ch. 17-18, pages 647-654, and 749-758, 1991.

[31] M. Podlogar, A. Recnik, G. Yilmazoglu, I. O. Ozer, M. Mazaj, E. Suvaci, and S. Bernik, “The Role of Hydrothermal Pathways in the Evolution of the Morphology of ZnO Crystals”, *Ceramics International*, Vol. 42, pages 15358-15366.

[32] S. Azizi, R. Mohamad, R. A. Rahim, A. B. Moghaddam, M. Moniri, A. Ariff, W. Z. Saad, and F. Namvab, “ZnO-Ag Core Shell Nanocomposite Formed by Green Method Using Essential Oil of Wild Ginger and their Bactericidal and Cytotoxic Effects”, *Applied Surface Science*, Vol. 384, pages 517-524, 2016.

[33] R. Bahramian, H. Eshghi, and A. Moshaii, “Influence of Annealing Temperature on Morphological, Optical and UV Detection Properties of ZnO Nanowires Grown by Chemical Bath Deposition”, *Materials and Design*, Vol. 107, pages 269-276.

[34] Polaron SC7620 sputter coater, Quorum Technologies, Lewes, United Kingdom, https://www.quorumtech.com/quorum-product/sc7620-mini-sputter-coaterglow-discharge-system.

[35] T. Zhang, W. Dong, M. Keeter-Brewer, S. Konar, R. N. Njabon, and Z. R. Tian, “Site-Specific Nucleation and Growth Kinetics in Hierarchical Nanosyntheses of Branched ZnO Crystallites”, *Journal of the American Chemical Society*, Vol. 128, No. 33, pages 10960-10968, 2006.

[36] Solar simulated light source, ABET Technologies Inc., 168 Old Gate Lane Milford, Connecticut 06460, http://abet-technologies.com/.

[37] Optical filter, Omega Optical Inc., 21 Omega Drive Brattleboro, VT 05301, http://www.omegafilters.com/.

[38] Z. Popovic and B. D. Popovic, “Introductory Electromagnetics”, *Prentice Hall, Inc.*, Version 12, pages 215-216, 2012.

[39] Z. Li, W. Zhong, X. Li, H. Zeng, G. Wang. W. Wang, Z. Yang, and Y. Zhang, “Strong room-temperature ferromagnetism of pure ZnO nanostructure arrays via colloidal template”, *Journal of Material Chemistry C*., Vol. 1, issue 41, pages 6807-6812, 2013.

[40] G. Wang, D. Chen, H. Zhang, J. Z. Zhang, and J. Li, “Tunable Photocurrent Spectrum in Well-Oriented Zinc Oxide Nanorod Arrays with Enhanced Photocatalytic Activity”, *Journal of Physical Chemistry C*, Vol. 112, No. 24, pages 8850-8855.

[41] Z-M. Liao, H.-Z. Zhang, and D.-P. Yu, “Ultralow-Frequency Photocurrent Oscillation in ZnO Nanowires”, *Applied Physics Letters*, Vol. 97, pages 033113-1-3, 2010.

[42] Mulia, C. M., Sathiaraj, T. S., and Maabong, K. “Effect of doping concentration on the properties of aluminium doped zinc oxide thin films prepared by spray pyrolysis for transparent electrode applications”. 2010. Ceramics International, Vol. 37, Issue 2. Pages 555-560.

[43] Schelonka, D., Tolasz, J., Vaclav, S. “Doping of Zinc Oxide with Selected First Row Transition Metals for Photocatalytic Applications”. 2015. Phorochemistry and Photobiology, Vol. 91, Issue 5. Pages 1071-1077.

Appendix A: Description of Research for Popular Publication

Zinc Oxide: The Secret Key to Unlocking a Better Tomorrow

In today's world, we like to brag that we know almost everything about the world around us. This is especially true when it comes to commonly understood scientific principles or the material used in today's electronics, such as silicon, germanium, or gallium arsenide. However, even in these areas where much research has been done and many facets of the materials properties are incredibly well known and controllable, there can lurk some unknown aspect or characteristic of said material. Once such material, zinc oxide, has been extensively researched and used over the past decade, often in sunscreen or white food dyes, and is being further researched for uses in solar cell or photo-detection technologies.

Zinc oxide, a semiconducting material, boasts possibly the broadest family of nanostructures known to science. The term "nanostructure" refers to materials which can be simple or very complex in shape, whose sizes fall within the nano (10^{-9} meters) scale. Typically, the electrical and optical properties of nanostructures will vary, given slight changes in nanostructure size or density, and even larger characteristic changes are exhibited between different structure shapes. Zinc oxide, a well-known absorber of ultraviolet light, can be grown in shapes called nano rods, wires, nails, tetrapods, ribbons, rings, springs, and many more; some, possibly unknown. Owing to the large number of available structures, the properties of zinc oxide as a nanomaterial are not all known or fully understood. Thus, much research is dedicated to working with different structures in order to discover or better understand these properties and find a unique use for them in today's electronics or optical devices.

One such research project, led by a team from the University of Arkansas, Fayetteville, is currently investigating a recently discovered nanostructure, which takes the shape of a single rod-like structure with spiked branches covering the exterior, which has been dubbed a "nanotree". These nanotrees are grown in between two electrodes sitting atop a clear quartz base, forming a simple ultraviolet photodetector. The new member in the zinc oxide family exhibits unusual properties when exposed to strong sun-like radiation and an electrical field. By subjecting the ultraviolet photodetector to a series of systematic experiments, each which have slightly varying conditions, the team aims to uncover the fundamental science behind the observed unusual properties, in the hopes of improving current solar or ultraviolet absorbing technology. This technology could pave the way for more efficient and cheap solar cells, which would help divert humanity away from it dependence on harmful and limited fossil fuels. Ultraviolet absorbing materials can also be used to enhance the resolution of space or ground based telescopes, giving humanity a clearer glimpse into the unknown wonders of our universe.

Appendix B: Executive Summary of Newly Created Intellectual Property

B.1. The photodetector with hydrothermally grown zinc oxide nanotrees, rods, or flowers, grown between interdigitated gold electrodes on a thin, single crystal quartz substrate, represents the intellectual property of the work done by the team which conducted the herein described research.

B.2. The custom 3D printed photodetector holder was designed specifically for the herein described research, and holds the device securely so that precise, controlled experiments can be run. Many slots in the central chamber allow the device to be placed in various locations within the holder for added experimental variability. Also, slide slots allow the addition of different sized magnets or other applicable instruments for experimentation. Finally, the central chamber is well sealed and painted to avoid excess light interference or reflection during the running of experiments, and also contains small slits which act as exits for wires attached to the contained device. The custom 3D blueprints represent the intellectual property of the work done by the team which conducted the herein described research.

Appendix C: Potential Patent and Commercialization Aspects of Listed Intellectual Property Items

C.1. Patentability of Intellectual Property

C.1.1. Zinc oxide nanostructured ultraviolet photodetector

Owing to the original design and usage of the specific zinc oxide nanostructures, a patent on the described photodetector could be filed.

C.1.2. Device Holder 3D Model

The device holder model was specific for the described research and represents intellectual efforts solely belonging to the team. Thus, this novel design has the potential for patent filing.

C.2. Commercialization Prospects

C.2.1. Zinc Oxide Nanostructured Ultraviolet Photodetector

The photodetecting device has a low potential for commercialization owing to its simplistic functionality.

C.2.2. Device Holder 3D Model

The device holder model could be patented and sold as a general purpose containing product with added security for controlled measurements and experimentation. However, due to the simplistic design and limited capabilities, the model has little commercial value.

C.3. Possible Prior Disclosure of IP

C.3.1. Zinc oxide Nanostructured Ultraviolet Photodetector

The photodetector, as it was detailed in this paper, has been described in conferences (ACS conference, Memphis TN, 2015) and other public presentations, although specific information regarding its construction were left undisclosed.

C.3.2. Device Holder 3D Model

The device holder, as it was detailed in this paper, has been referred to in public presentations, but no detailed information was disclosed.

Appendix D: Broader Impact of Research

D.1. Applicability of Research Methods to other Problems

The systematic experimental methods used in this research can be applied to any similarly related optoelectronic device. The addition of single variables and measuring of any observed changes during an experiment can potentially help uncover certain traits of those devices. In the case of any photodetector, the methods use in this research would likely prove useful and informative.

D.2. Impact of Research Results of US and Global Society

The results of this research can provide information pertaining to scientific areas such as optics, electronics, semiconductors, and surface physics. Possibly most important from this list is semiconductors and their properties. Semiconductors are used extensively in today's technology and devices. Most every human on Earth is connected via computers and the internet, whose functionality is almost completely dependent on the operation of semiconductors. Major companies and countries which produce the integrated circuits that run today's electronics are always seeking out new materials or properties to take advantage of in order to yield the most efficiency and functionality of those electronics. Zinc oxide as a semiconductor has such a large family of nanostructures, and has already found a use in the optoelectronics field, but further research is still needed to maximize this usefulness. The results of the research point to properties of zinc oxide useful for photodetection, atmospheric sensing, and light blocking, but the results also indicate the possible existence of useful phenomena in other fields.

D.3. Impact of Research Results on the Environment

Scientific progress should always be wary of its effects on the environment, otherwise the very efforts to improve humanity's future could be done in ways which compromise it. It was always the goal of the described research to be conducted in a way and using such materials which did not pose a significant threat to the environment. Zinc oxide was primarily chosen for this reason, as it is generally bio-safe and abundant. Also, as zinc oxide is an ultraviolet absorber, it has been used in many different types of solar cells, which seek to provide cheap, renewable energy for today and the future.

Appendix E: Microsoft Project

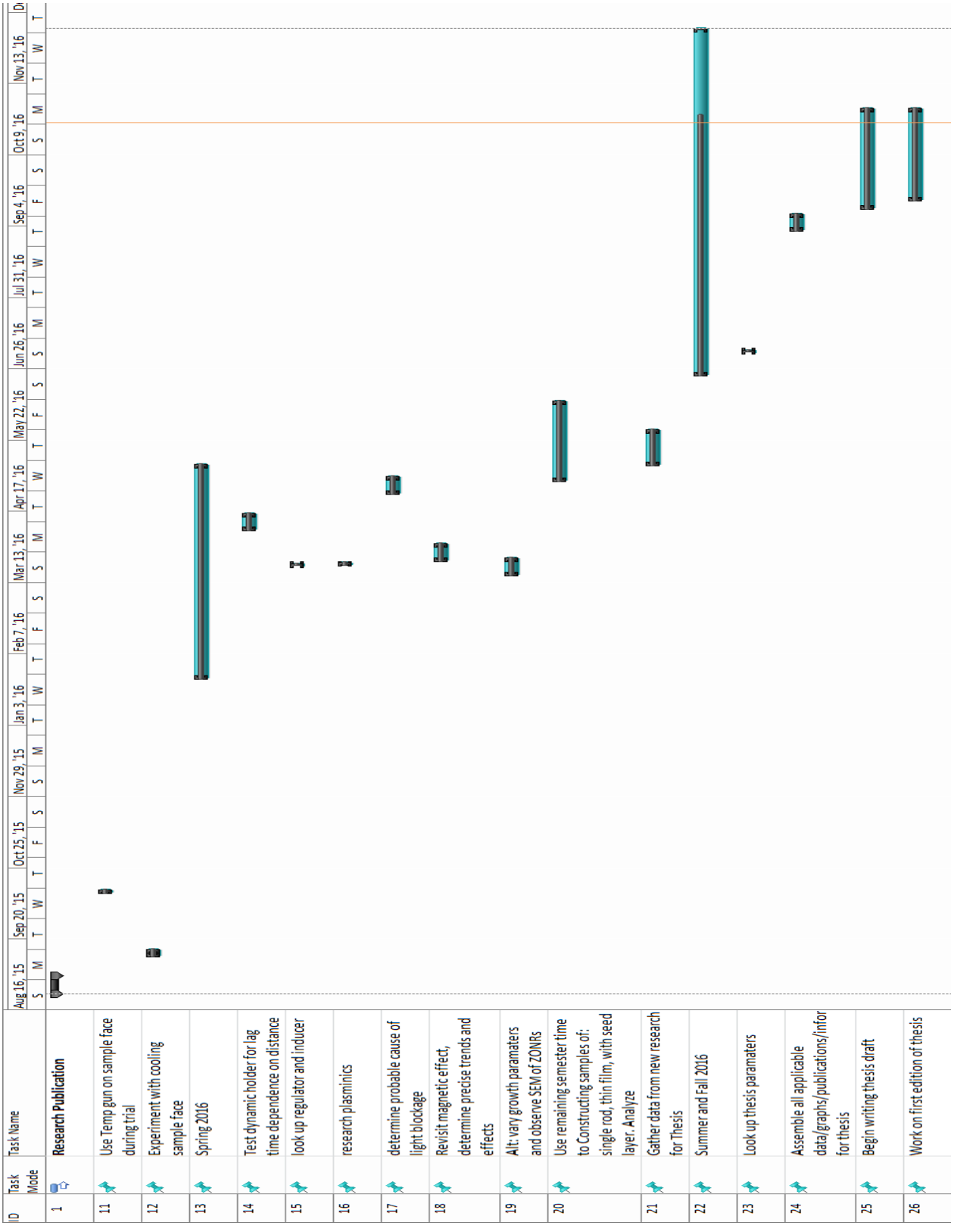

ID	Task Mode	Task Name
27		Apply to grad
28		Send first edition to Tian for review
29		revise 2nd edition
30		Submit abstract, title, and other info to MEP office
31		Tian final approval
32		Send to thesis committee for review
33		Final draft
34		Public presentation
35		Masters defense
36		Submit thesis and all important documentation for
37		Graduate!

Appendix F: Identification of Hardware and Software in Research and Thesis Writing

Computer #1:

Model Number: MS-16GF MSI Apache GE 2PC

Serial Number: 2PC-469USK140000116

Owner: Garrett Torix

Software #1

Name: Microsoft Office 2016

Owner: Garrett Torix

Computer #2:

Model Number: DCSM1F Dell Optiplex 780

Serial Number: 1ST3WN1

Location: DISC 217 University of Arkansas

Owner: Department of Chemistry and Biochemistry, University of Arkansas

Software #2:

Name: CHI660B Electrochemical Workstation

Owner: Department of Chemistry and Biochemistry, University of Arkansas

Appendix G: All Publications Published, Submitted, and Planned

Garrett Torix, Tyler Chism, Dr. Ryan Tian. "Investigation of Optical and Electrical Characteristics in Zinc Oxide Branched Nano-structures". Planned for publication.